International Journal of Solids and Structures 50 (2013) 429–446

Contents lists available at SciVerse ScienceDirect

International Journal of Solids and Structures

journal homepage: www.elsevier.com/locate/ijsolstr

Optimal topological design through insertion and configuration of finite-sized heterogeneities

Hung-Yun Lin, Ganesh Subbarayan *

School of Mechanical Engineering, Purdue University, West Lafayette, IN 47907, United States

ARTICLE INFO

Article history:
Received 24 February 2012
Received in revised form 24 September 2012
Available online 23 October 2012

Keywords:
Topology optimization
Shape optimization
Configuration optimization
Configurational derivative

ABSTRACT

In this paper, we develop a procedure for optimal topological design by sequentially inserting *finite-sized non-spherical inclusions or holes* within a homogeneous domain. We propose a new criterion for topology change that results in a trade-off problem to achieve the greatest/least change in the objective for the least/greatest change in the size of the inclusion/hole respectively. We derive the material derivative of the proposed objective, termed as the configurational derivative, that describes sensitivity of arbitrary functionals to arbitrary motions of the inclusion/hole as well as the domain boundaries. We specifically utilize the sensitivity to position, orientation and scaling of finite-sized heterogeneities to effect topological design. We simplify the configurational derivative to the special case of infinitesimally small spherical inclusions or holes and show that the developed derivative is a generalization of the classical topological derivative. The computational implementation relies on B-spline isogeometric approximations. We demonstrate, through a series of examples, optimal topology achieved through sequential insertion of a heterogeneity of fixed shape and optimization of its configuration (location, orientation and scale).

1. Introduction

Often in engineering practice, there is a need to perform optimal topological design by placing *finite-sized, regular-shaped* geometries within the structure. Classically, topological design of structures is achieved by optimally distributing material in a fixed region with known loading and boundary conditions (Bendsoe and Sigmund, 2003). One commonly applied strategy for topology optimization is to consider the material as having a varying density in the range $[0,1]$, which at the lower limit results in a void. Another approach to topology optimization is through homogenization of periodic media, where the microstructure at each point in the design space is optimized (Bendsoe and Sigmund, 2003). Shape optimal design (see Pironneau, 1984; Bennett and Botkin, 1986), in contrast to topology optimization, is concerned with determining the optimal boundary shapes of (typically homogeneous) objects that satisfy criteria such as minimum mass. Efforts at integrating topology and shape optimization have often focused on automating the transition between them (see for example Lin and Chao, 2000; Tang and Chang, 2001; Ansola et al., 2002).

In practice, the efficiency of topology and shape optimal design procedures is strongly dependent on the availability of analytically derived domain and shape design sensitivities (Dems and Mroz, 1983, 1984; Haug et al., 1986; Sokolowski and Zolesio, 1992) and their implementation in a finite element code. Therefore, the derivation of these sensitivities is a critical aspect of topology and shape optimal design.

Instead of topological design by distributing material optimally within the domain, an alternative approach to effecting topological modifications in the literature is by introducing infinitesimal holes and subsequently optimizing their size and shape. In spirit, this approach resembles shape optimal design. The advantages of such an approach include procedural unification of topology and shape optimization, greater control over resulting topologies and shapes, an ability to handle geometrical constraints imposed by manufacturing process, and smaller number of design variables leading to greater computational efficiency.

In an early study, Eschenauer et al. (1994) developed the "bubble method," in which the conditions for introducing an infinitesimal hole into the structure was derived. The hole was subsequently parameterized using NURBS basis functions, the structure meshed using finite elements, analyzed, leading eventually to the optimized hole shape. This procedure was applied iteratively leading to a sequential procedure for topological modification. More recently, the bubble method has been extended as the "bubble-and-grain" method through conditions for introduction planar, elliptical, infinitesimal inclusions for the strain energy density objective (Kobelev, 2010).

The generalization of the bubble method for introduction of infinitesimal spherical holes in the domain is through the notion of topological derivative (Sokolowski and Zochowski, 1999; Cea

* Corresponding author. Tel./fax: +1 7654949770.
E-mail address: ganeshs@purdue.edu (G. Subbarayan).

0020-7683/$ - see front matter © 2012 Elsevier Ltd. All rights reserved.
http://dx.doi.org/10.1016/j.ijsolstr.2012.10.006

et al., 2000). The topological derivative is an estimate of the change in shape functionals due to introduction of infinitesimal spherical holes in the interior of the domain. To overcome the assumptions on the nature of the cost functions and the boundary conditions imposed on the introduced holes, an alternative definition of topological derivative corresponding to an expanding spherical hole in the spirit of shape sensitivity analysis was introduced by Novotny et al. (2003). In the limit when the hole radius asymptotically approached zero, the alternative definition of sensitivity led to the usual definition of topological sensitivity as the sensitivity corresponding to creation of a hole. Further, the topological derivative has also been extended to introduction of infinitesimal ellipsoidal inclusions (Cedio-Fengya et al., 1998; Nazarov and Sokolowski, 2003; Ammari and Kang, 2005; Amstutz, 2006).

In general, the topological derivative does not lend itself to introduction and modification of *finite-sized heterogeneities*. There are very few studies that appear to have explored the effect of introducing finite-sized heterogeneities on *arbitrary functionals* defined over the domain. In Gopalakrishnan and Suresh (2008), the authors develop the notion of feature sensitivity wherein the effect of introducing a finite-sized hole parameterized using a scalar feature (or scaling) parameter in the range [0,1] was estimated. The feature sensitivity was then used to explore the impact of finite-sized hole introduced at various locations within the domain, i.e., to enable "fast reanalysis." The procedure also necessitated a solution to an exterior boundary value problem of a finite-sized hole placed in an infinite domain.

Optimal topological design through introduction of finite-sized inclusions or holes into homogeneous domains will in general require sensitivities of *arbitrary functionals* to changes in position, orientation or scaling. Such sensitivities of arbitrary functionals appear to be uncommon in the literature, and seem to have been explored only in Dems and Mroz (1986) in the context of deriving conservation rules, or path independent integrals, within solids that are *homogeneous* except for a crack or a void. Although such conservation rules have played a critical role in the field of fracture mechanics (see for instance, Eshelby, 1956; Rice, 1968; Knowles and Sternberg, 1972; Budiansky and Rice, 1973), the sensitivities of arbitrary functionals to translation, rotation and scaling do not appear to have been heretofore exploited for optimal topological design.

Finally, from a numerical solution perspective, the need to remesh domains with evolving inclusion/hole shapes remains a significant challenge. Therefore, *numerical examples based on arbitrary topological modifications effected by insertion and growth of an explicitly defined heterogeneity* have been relatively few in the literature.

Based on the above survey of literature, the goal of this paper is to demonstrate optimal topological design through insertion and configuration of finite-sized holes and inclusions by

1. Identifying a criterion and its material time derivative that provides sensitivity to the configuration (location, orientation and scale) of both "soft" as well as "stiff" finite-sized inclusions.
2. Showing that simplification of the material derivative to infinitesimal, spherical inclusions results in the classical topological derivative.
3. Illustrating through a series of examples the approach to effecting optimal topology by sequentially inserting, orienting and scaling finite-sized inclusions and contrasting the resulting optimal design to those obtained by placing infinitesimal heterogenieties.

2. Configurational derivative and optimal location, orientation and scaling conditions

In this section, we derive the necessary conditions to determine the optimal configuration of an inclusion within a homogeneous domain whose boundaries evolve in time. In particular, we permit both the inclusion boundary as well as the underlying matrix boundary to evolve. The optimal configuration of the inclusion is determined by solving the problem described below.

2.1. The configuration optimization problem

Given a domain Ω we describe a "design transformation" that is continuous with the pseudo "design time" t within the domain such that

$$\mathbf{x} = \mathbf{x}(\mathbf{X}, t) \tag{1}$$

where $\mathbf{X}$ is initial position in the domain independent of time and Ω denotes the configuration at any time instant t. Also, Γ denotes the boundary of the domain Ω. We define Ω^{t_0} as the initial configuration. As with $\mathbf{X}$, Ω^{t_0} is assumed independent of time. Associated with this design "deformation," a "design velocity" may now be defined as:

$$\mathbf{v}(\mathbf{x}, t) = \frac{\partial \mathbf{x}}{\partial t} \tag{2}$$

We now generalize the above body by introducing a heterogeneity defined over Ω_p bounded by Γ_p (see Fig. 1) located at position $\mathbf{x}_p$ inside the domain Ω. We define an objective over this heterogeneous domain as:

$$f(t) = \int_\Omega \psi \, d\Omega \tag{3}$$

where $\psi \equiv \psi(\varepsilon(\mathbf{x}(t)), \mathbf{x}(t), t)$ is the value of the design criterion at instant t. Henceforth, we will suppress the arguments of ψ for ease of reading. The corresponding quantity in the homogeneous domain is ψ^0. We associate with the inclusion and outside of it densities $\rho(\mathbf{x}(t), t)$ and $\rho^0(\mathbf{x}(t), t)$ respectively. In other words, outside of the inclusion, the density in the domain is the same as that in the homogeneous domain. In general, we permit the inclusion to be either "stiff" ($\rho > \rho^0$ in Ω_p and $\psi < \psi^0$ in $\Omega - \Omega_p$) or "soft" ($\rho < \rho^0$ in Ω_p and $\psi > \psi^0$ in $\Omega - \Omega_p$).

The goal of the configuration optimization problem is to optimally determine the reference location $\mathbf{x}_p$ of the inclusion, the orientation $\mathbf{n}_p$ of a reference axis passing through $\mathbf{x}_p$, and a rotation θ about the reference axis as well as the inclusion shape to achieve the greatest/least "effect" for the least/greatest change in mass of a stiff/soft inclusion. Thus, we formally pose the *configuration optimization problem* as the following trade-off optimization problem: find $\mathbf{x}_p, \mathbf{n}_p, \theta$ and the optimized inclusion shape to

$$\begin{aligned} &\text{minimize} \quad g(t) = \pm \int_\Omega (\psi - \psi^0) d\Omega + w \int_\Omega (\rho - \rho^0) d\Omega \\ &\text{Subject to} \int_\Omega \varepsilon : \mathbf{C} : \varepsilon^a d\Omega - \int_\Gamma \mathbf{t} \cdot \mathbf{u}^a d\Gamma = 0 \\ &\qquad \int_\Omega \varepsilon^0 : \mathbf{C}^0 : \varepsilon^{a0} d\Omega - \int_\Gamma \mathbf{t}^0 \cdot \mathbf{u}^{a0} d\Gamma = 0 \end{aligned} \tag{4}$$

where the positive sign on the objective applies for a stiff inclusion, and the negative sign for a soft inclusion; $\varepsilon^a(\mathbf{x}(t))$ and $\mathbf{u}^a(\mathbf{x}(t))$ are compatible virtual strains and displacements respectively. Similarly, $\varepsilon^{a0}(\mathbf{x}(t))$ and $\mathbf{u}^{a0}(\mathbf{x}(t))$ are corresponding virtual quantities in the homogeneous domain; $\mathbf{t}$ and $\mathbf{t}^0$ are the tractions on the boundary of the domains (assumed unchanging with time) with and without the inclusion respectively. $\mathbf{C}$ and $\mathbf{C}^0$ are the fourth rank elasticity tensors (assumed constant with time) in the inhomogeneous and homogeneous domains. Implicit in the above statement is the fact that on the portion of the boundary Γ_u where displacement boundary conditions are applied, $\mathbf{u}^a = \mathbf{u}^{a0} = 0$. Γ_t is the portion of boundary where tractions are prescribed, and $\Gamma = \Gamma_u \cup \Gamma_t$. The body forces are ignored in the constraints corresponding to the principle of virtual work for convenience. We show that by imposing the virtual

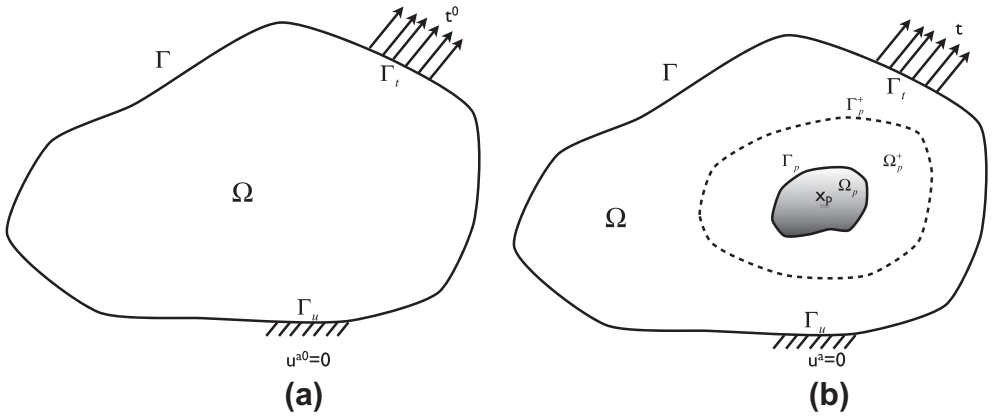

Fig. 1. Illustrations of homogeneous and heterogeneous domains.

work statement as a constraint, the adjoint boundary value problems naturally emerge.

The value of the weight $w \in [0,\infty]$ represents the relative preference for the two terms in the objective. The weight w may also be alternatively expressed as $w = \frac{\bar{w}}{(1-\bar{w})}\frac{\bar{\psi}}{\bar{\rho}}$ with $\bar{w} \in [0,1]$, and with $\bar{\psi}$ and $\bar{\rho}$ being scaling constants on ψ and ρ respectively. In general, the weight value has a one-to-one correspondence with the maximum allowable mass change in the case of a stiff inclusion (or minimum required in the case of a soft inclusion). It is possible that an optimal solution may not exist for an arbitrarily chosen weight since the mass change corresponding to a chosen weight may be unachievable. Also, if a fixed size inclusion is translated or rotated within the domain, then the rate of change of mass of the body is zero, and therefore the term involving densities in the objective becomes irrelevant for an inclusion of fixed shape as we show later.

The reference to the homogeneous domain in the objective needs elaboration. Without this reference, arguably, the form of the objective in the presence of a stiff/soft inclusion will be non-obvious. In fact, we show later that without the homogeneous terms, the objective does not accurately determine the sizes of stiff *as well as* soft inclusions for a chosen weight $\bar{w}$.

We now recognize that the design velocities $\mathbf{v}$ and $\mathbf{v^0}$ in the inhomogeneous and homogeneous domains respectively are arbitrary and define design intent to move the boundaries of the body. Therefore, we impose the conditions implicit and natural in the statement of Problem (4), namely, $\mathbf{v} = \mathbf{v^0}$ in Ω and $\mathbf{t} = \mathbf{t^0}$ on Γ_t.

2.2. The configurational derivative

We derive next the material derivative of the objective in Problem (4), that yields the configurational derivative when the constraints corresponding to virtual work are satisfied. For convenience of derivation, we will consider the objective with the positive sign corresponding to a stiff inclusion while carrying out the derivation, and distinguish the appropriate sign for stiff/soft inclusion in the final result.

The Lagrangian corresponding to Problem (4) is:

$$\begin{aligned} G(t) = {} & \int_\Omega \psi d\Omega - \left(\int_\Omega \varepsilon : \mathbf{C} : \varepsilon^a d\Omega - \int_\Gamma \mathbf{t}\cdot\mathbf{u}^a d\Gamma \right) - \int_\Omega \psi^0 d\Omega \\ & + \left(\int_\Omega \varepsilon^0 : \mathbf{C^0} : \varepsilon^{a0} d\Omega - \int_\Gamma \mathbf{t}\cdot\mathbf{u}^{a0} d\Gamma \right) + w \\ & \times \int_\Omega (\rho - \rho^0) d\Omega \end{aligned} \tag{5}$$

We derive in Appendix A, using established procedures (Malvern, 1969; Arora, 1993), the material time derivative of Lagrangian $G(t)$ as:

$$\begin{aligned} \dot{G}(t) = {} & \int_\Omega \frac{\partial}{\partial t}(\psi - \psi^0) d\Omega + w \int_{\Omega_p} \frac{\partial}{\partial t}(\rho - \rho^0) d\Omega \\ & + \int_{\Gamma_p} [[(\psi + w\rho)(\mathbf{n}\cdot\mathbf{v})]] d\Gamma \\ & - \left(\int_\Omega (\varepsilon : \mathbf{C} : \varepsilon^a - \varepsilon^0 : \mathbf{C^0} : \varepsilon^{a0})(\nabla\cdot\mathbf{v})\, d\Omega \right. \\ & \left. - \int_{\Gamma_t} (\mathbf{t}\cdot\mathbf{u}^a - \mathbf{t}^0\cdot\mathbf{u}^{a0})(\nabla\cdot\mathbf{v}) d\Gamma \right) \\ & - \int_{\Gamma_t} (\mathbf{t}\cdot\mathbf{u}^a - \mathbf{t}^0\cdot\mathbf{u}^{a0})(\mathbf{n}\cdot\nabla\mathbf{v}\cdot\mathbf{n}) d\Gamma \end{aligned} \tag{6}$$

The above derivation relies on the following adjoint problems defined in inhomogeneous and homogeneous domains, respectively:

$$\int_\Omega \dot{\varepsilon} : \mathbf{C} : \varepsilon^a \, d\Omega - \int_\Gamma \mathbf{t}^a \cdot \dot{\mathbf{u}} \, d\Gamma = 0 \tag{7}$$

$$\int_\Omega \dot{\varepsilon}^0 : \mathbf{C^0} : \varepsilon^{a0} \, d\Omega - \int_\Gamma \mathbf{t}^{a0} \cdot \dot{\mathbf{u}}^0 \, d\Gamma = 0 \tag{8}$$

with $\mathbf{t}^a \cdot \nabla\mathbf{u}^T \cdot \mathbf{n} = \psi$ and $\mathbf{t}^{a0} \cdot \nabla\mathbf{u}^{0T} \cdot \mathbf{n} = \psi^0$ on Γ_t. $G(t)$ reaches its extreme value, i.e., the above material derivative is zero at the optimum. We define the material derivative as the *configurational derivative*. In general, to evaluate the configurational derivative we need to solve four boundary value problems: (1) original problem in the inhomogeneous domain, (2) adjoint problem in the inhomogeneous domain, (3) original problem in the homogeneous domain and (4) adjoint problem in the homogeneous domain.

Commonly, the design objective as well as the density does not possess explicit design time dependence. Under these restrictions, and generalizing the derivation for both stiff and soft inclusions, Eq. (6) reduces to:

$$\begin{aligned} \dot{G}(t) = \pm \Bigg[& \int_{\Gamma_p} [[(\psi \pm w\rho)(\mathbf{n}\cdot\mathbf{v})]] d\Gamma \\ & - \left(\int_\Omega (\varepsilon : \mathbf{C} : \varepsilon^a - \varepsilon^0 : \mathbf{C^0} : \varepsilon^{a0})(\nabla\cdot\mathbf{v})\, d\Omega \right. \\ & \left. - \int_{\Gamma_t} (\mathbf{t}\cdot\mathbf{u}^a - \mathbf{t}^0\cdot\mathbf{u}^{a0})(\nabla\cdot\mathbf{v}) d\Gamma \right) \\ & - \int_{\Gamma_t} \mathbf{t}\cdot(\mathbf{u}^a - \mathbf{u}^{a0})(\mathbf{n}\cdot\nabla\mathbf{v}\cdot\mathbf{n}) d\Gamma \Bigg] \end{aligned} \tag{9}$$

where the positive sign applies for a stiff inclusion and the negative sign for a soft inclusion. We have also used the fact that $\mathbf{t} = \mathbf{t}^0$ on Γ_t in the last line. As mentioned earlier, $\mathbf{v}$ is an *arbitrarily defined* velocity dictated by design intent.

2.3. Optimality conditions for location, orientation and scaling of an inclusion

We now consider three specific transformations corresponding to translation, rotation and uniform scaling of domain Ω:

$$\mathbf{v} = \hat{\mathbf{v}} \tag{10}$$

$$\mathbf{v} = \boldsymbol{\omega} \times \mathbf{r} \tag{11}$$

$$\mathbf{v} = \alpha(t)\mathbf{r} \tag{12}$$

where $\hat{\mathbf{v}}$ is a (spatially) constant velocity, $\boldsymbol{\omega}$ is a constant angular velocity about an arbitrary axis oriented along $\mathbf{n}_p$ passing through an arbitrary point $\mathbf{x}_p$ with $\mathbf{r} = \mathbf{x} - \mathbf{x}_p$, and $\alpha(t)$ is a parameter, independent of spatial location, defining the scaling of the inclusion relative to an arbitrary point $\mathbf{x}_p$. Under the first two transformations, $\nabla \cdot \mathbf{v}$ trivially vanishes ($\nabla \cdot \boldsymbol{\omega} \times \mathbf{r} = \nabla \times \boldsymbol{\omega} \cdot \mathbf{r} - \boldsymbol{\omega} \cdot \nabla \times \mathbf{r}, \nabla \times \mathbf{r} = 0$ and $\nabla \times \boldsymbol{\omega} = 0$), while $\nabla \cdot \mathbf{v} = d\alpha$ under scaling with d being the dimension of the problem (2 or 3). Thus, under all three transformations, the following condition is satisfied either trivially or on account of the required equilibrium condition in Problem (4):

$$\int_\Omega (\varepsilon : \mathbf{C} : \varepsilon^a - \varepsilon^0 : \mathbf{C}^0 : \varepsilon^{a0})(\nabla \cdot \mathbf{v})\, d\Omega - \int_{\Gamma_t} (\mathbf{t} \cdot \mathbf{u}^a - \mathbf{t}^0 \cdot \mathbf{u}^{a0})(\nabla \cdot \mathbf{v}) d\Gamma = 0 \tag{13}$$

Thus, under the above three transformations, the configurational derivative, Eq. (9), takes the respective forms:

$$\dot{G}(t) = \pm \left[\int_{\Gamma_p} [[(\psi \pm w\rho)\mathbf{n}]] d\Gamma \right] \cdot \hat{\mathbf{v}} \tag{14}$$

$$\dot{G}(t) = \pm \left[\int_{\Gamma_p} [[(\psi \pm w\rho)(\mathbf{r} \times \mathbf{n})]] d\Gamma \right] \cdot \boldsymbol{\omega} \tag{15}$$

$$\dot{G}(t) = \pm \left[\int_{\Gamma_p} [[(\psi \pm w\rho)(\mathbf{r} \cdot \mathbf{n})]] d\Gamma - \int_{\Gamma_t} \mathbf{t} \cdot (\mathbf{u}^a - \mathbf{u}^{a0}) d\Gamma \right] \alpha(t) \tag{16}$$

where we have used $\mathbf{n} \cdot \nabla(\boldsymbol{\omega} \times \mathbf{r}) \cdot \mathbf{n} = \mathbf{n} \times \mathbf{n} \cdot \boldsymbol{\omega} = 0$ and $\mathbf{n} \cdot \nabla(\alpha \mathbf{r}) \cdot \mathbf{n} = \alpha$. In the above conditions, if ρ is constant on Γ_p, then the density term drops out of Eq. (14) and Eq. (15) since $\int_{\Gamma_p} \mathbf{n} d\Gamma = 0$ and $\int_{\Gamma_p} \mathbf{r} \times \mathbf{n} d\Gamma = 0$. Also, for a spherical inclusion, Eq. (15) is trivially satisfied if the sphere is centered on $\mathbf{x}_p$ since then $\mathbf{r} \times \mathbf{n} = 0$.

Evaluating Eqs. (14) and (15) require only the solution to the original boundary value problem corresponding to the heterogeneous domain. To evaluate Eq. (16), on the other hand, the original and adjoint boundary value problems on the heterogeneous domain and the adjoint boundary value problem on the homogeneous domain need to be solved. Also, excluding the homogeneous terms in Problem (4) will not alter the conditions of Eqs. (14) and (15), but will eliminate the $\mathbf{u}^{a0}$ term alone in Eq. (16). Thus, clearly, adding the homogeneous terms in the objective is necessary in Eq. (16) to discern the effect of inclusion boundary motion relative to the domain boundary motion. More importantly, the sign of the sensitivity needs to change between soft and stiff inclusions. Such a change in the sign does not occur in the absence of the homogeneous terms in the objective.

It is possible to derive an alternative form for Eq. (16) (see Appendix B) as an integral on the boundary of the inclusion by a procedure inspired by the derivation of the Eshelby formula (Eshelby, 1956; Christensen, 2005):

$$\dot{G}(t) = \pm \left[\int_{\Gamma_p} [[(\psi \pm w\rho)(\mathbf{r} \cdot \mathbf{n})]] d\Gamma - \int_{\Gamma_p^+} (\mathbf{t}^{a0} \cdot \mathbf{u} - \mathbf{t} \cdot \mathbf{u}^{a0}) d\Gamma - \int_\Gamma (\mathbf{t}^a - \mathbf{t}^{a0}) \cdot \mathbf{u}\, d\Gamma \right] \alpha(t) \tag{17}$$

While, in general, $\mathbf{t}^a \neq \mathbf{t}^{a0}$ on Γ_t, for the most common objective used in topology optimization $\psi = \sigma : \varepsilon$, as discussed in the following section, $\mathbf{t}^a = \mathbf{t} = \mathbf{t}^0 = \mathbf{t}^{a0}$ on Γ_t, and, if the boundary condition is such that $\mathbf{u} = 0$ on Γ_u, then the last integral vanishes. It should be noted that the surface Γ_p^+ in the above expression is arbitrary, and dictated more by convenience of evaluation. Two relevant choices for Γ_p^+ are the inclusion boundary Γ_p, or the domain boundary Γ.

There are at least three uses for the configurational derivative described by Eqs. (6), (14)–(17):

1. Provide the optimality criterion for placing, orienting or scaling the inclusion ($\dot{G}(t) = 0$). However, it is important to note that such an extremum may not exist within the domain Ω.
2. Algorithmically enable iterative search for the optimal inclusion location, orientation, or size by identifying the search direction that produces the steepest gradient in the objective. Thus, the steepest descent/ascent direction at instant t identified from Eqs. (14)–(17) are $\mathbf{d} = -\dot{G}(t)$.
3. Estimate the impact of arbitrarily modifying the shape of the inclusion as well as the domain (i.e., for shape design sensitivity).

2.4. Simplification based on choice of objective

In the examples illustrated later in the present paper, we will use the criterion that is most common for topological modification (Bendsoe and Sigmund, 2003), one that is related to the structural compliance. Specifically, we will use:

$$\psi(\varepsilon(\mathbf{x}(t)), \mathbf{x}(t), t) = \sigma : \varepsilon \tag{18}$$

Thus, from the definition of the adjoint tractions stated earlier (see also Eq. (32) of Appendix A), we get:

$$\mathbf{t}^a = \sigma \cdot \mathbf{n} \quad \text{on} \quad \Gamma_t \tag{19}$$

Therefore, the adjoint boundary value problem is deduced to be identical to the original boundary value problem. In this case, the adjoint boundary value problem is trivially eliminated by setting $\varepsilon^a = \varepsilon$ everywhere in Ω. By the same argument as above, the adjoint problem is avoided in the homogeneous domain with its corresponding objective ψ^0 as well.

2.5. Simplification for optimal location of an infinitesimal spherical particle

We consider now a spherical inclusion of radius R centered at $\mathbf{x}_p$. As discussed earlier, for the most common objective used in topology optimization $\psi = \sigma : \varepsilon, \mathbf{t}^a = \mathbf{t} = \mathbf{t}^0 = \mathbf{t}^{a0}$ on Γ_t. Therefore, the solutions to the original and adjoint problems are identical for this specific objective. Thus, the scaling sensitivity described by Eq. (16) becomes for this objective:

$$\dot{G}(t) = \pm \left[\int_{\Gamma_p} [[(\psi \pm w\rho)(\mathbf{r} \cdot \mathbf{n})]] d\Gamma - \int_{\Gamma_t} \mathbf{t} \cdot (\mathbf{u} - \mathbf{u}^0) d\Gamma \right] \alpha(t) \tag{20}$$

where we have introduced a positive scaling rate $\alpha(t)$. If the inclusion is an infinitesimal spherical particle, the last integral in the above expression may be ignored since the perturbation caused by the inclusion is local. Thus, for the chosen objective, in the event of an infinitesimal spherical inclusion of radius R

$$\dot{G}(t) = \pm \left[\int_{\Gamma_p} \left[(\psi^- - \psi^+) \pm w(\rho^- - \rho^+) \right] d\Gamma \right] R\alpha(t) \tag{21}$$

where $(\cdot)^-/(\cdot)^+$ refer to quantities just inside/outside the inclusion boundary Γ_p respectively, $\mathbf{n} = \mathbf{n}^- = -\mathbf{n}^+$ is the outward normal to the inclusion boundary. We have also made use of the fact that $\mathbf{r} = R\mathbf{n}$ on the spherical surface. Using well established ideas from the field of micromechanics (Nemat-Nasser and Hori, 1999), assuming that the elastic tensors $\mathbf{C}$ and $\mathbf{C}^0$ are isotropic, we derive in

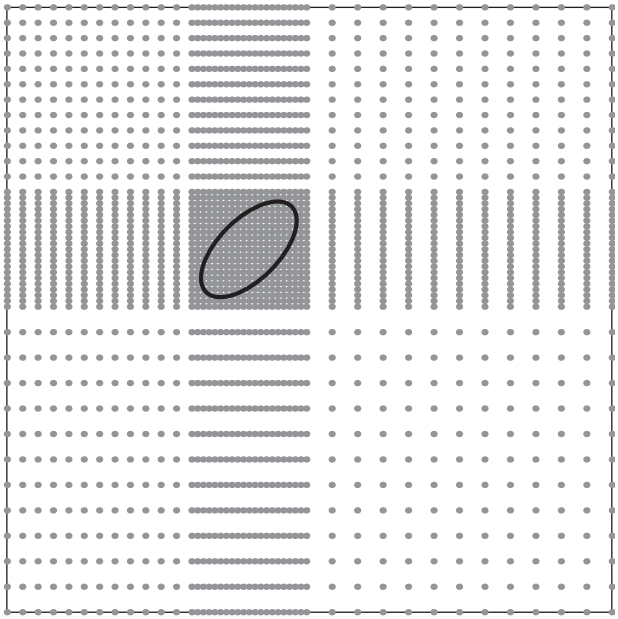

Fig. 2. Illustration of the refined control net automatically generated by the developed program in the vicinity of elliptical features.

Appendix C, the expression for the integral of the jump in objective ψ in Eq. (21) in terms of the elasticity tensors as well as the applied strain field ε^0 as:

$$\int_{\Gamma_p} (\psi^- - \psi^+)\, d\Gamma = -\left(\varepsilon^0 : \hat{\mathbf{C}} : \varepsilon^0\right)\Gamma_p \tag{22}$$

where $\Gamma_p = 4\pi R^2$ and the tensor $\hat{\mathbf{C}}$ is of the form $\hat{\mathbf{C}}_{ijkl} = c_1\delta_{ij}\delta_{kl} + c_2(\delta_{ik}\delta_{jl} + \delta_{il}\delta_{jk})$ with the coefficients c_1 and c_2 as defined in Appendix C. Thus, using this result, the sensitivity of Eq. (21) reduces to:

$$\dot{G}(t) = \left[\mp\varepsilon^0 : \hat{\mathbf{C}} : \varepsilon^0 + w(\rho^- - \rho^+)\right]\Gamma_p v_n \tag{23}$$

since the velocity normal to the spherical inclusion boundary is $v_n = R\alpha(t)$. In the limit of infinitesimal inclusion, we define the topological derivative as the quantity within the square brackets:

$$D_T(\mathbf{x}_p) = \mp\varepsilon^0(\mathbf{x}_p) : \hat{\mathbf{C}} : \varepsilon^0(\mathbf{x}_p) + w(\rho^- - \rho^+) \tag{24}$$

where, as before, the first sign preceding the expression corresponds to the stiff inclusion and the second to the soft inclusion. Finally, the optimal spatial location, $\mathbf{x}_p$ for the insertion of the inclusion is given by the condition:

$$\nabla D_T(\mathbf{x}_p) = \mp 2\nabla\varepsilon^0(\mathbf{x}_p) : \hat{\mathbf{C}} : \varepsilon^0(\mathbf{x}_p) = 0 \tag{25}$$

Ignoring the trivial case when the inclusion is of the same material as the matrix material (i.e., when $c_1 = c_2 = 0$), the optimal location is one where either the strain is zero or the spatial gradient of the strain is zero. Clearly, at such locations, the objective $\psi^0 = \varepsilon^0 : \mathbf{C}^0 : \varepsilon^0$ achieves an extreme value as well.

3. Numerical implementation

A significant challenge to topology optimization through heterogeneity insertion and growth is the evaluation of the criterion that determines the heterogeneity location, and the boundary optimization following the heterogeneity insertion. Both of these steps have in the past required meshing of the sequentially modified domain followed by finite element analysis. Therefore, any scheme that obviates the need for remeshing while retaining the advantages of heterogeneity introduction stated above is likely to be efficient for topological optimization.

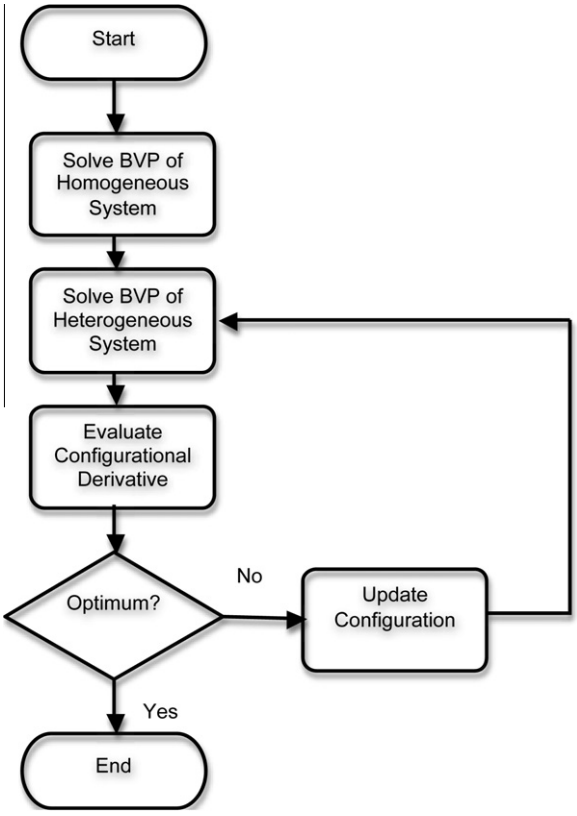

Fig. 3. Flow of control during the execution of the code.

In the numerical implementation of configurational derivative demonstrated in this paper, we follow the hierarchical partition of unity field compositions (HPFC) procedure developed by the authors Natekar et al., 2004; Zhang and Subbarayan, 2004, 2006; Zhang et al., 2007; Rayasam et al., 2007a,b. In the examples, a "dominated" union in which the weight of the composed field corresponding to the inclusion is unity and the corresponding weight of the underlying homogeneous field is zero is used. In the present study, the underlying homogeneous field as well as the composed field corresponding to the heterogeneity are approximated by B-Splines. Both the polynomial B-Splines as well as the rational Non-Uniform Rational B-Splines (NURBS) are very popular choices in CAD as well as isogeometric analysis (Renken, 1997, 2000; Kagan and Fischer, 2000; Natekar et al., 2004; Hughes et al., 2005; Rayasam et al., 2007a). The procedure is implemented using Mathematica®, a computer algebra system (CAS) that enables symbolic operations as well as higher-level programming. The developed program contained 1000 lines of Mathematica code. Since the examples discussed below contain stress-concentrating elliptical inclusions or voids, a refined control net distribution in the neighborhood of heterogeneity boundary was necessary to accurately capture the stress state. Therefore, an automatic procedure to adaptively generate a net of 45×45 control points around the heterogeneity at any design state was developed, as shown in Fig. 2. On an average, the analysis took 73 s to complete one iteration on a desktop machine powered by a 2.4 GHz Intel Core 2 Duo processor. During the analysis, the boundary value problem of homogeneous system corresponding to the reference design state was solved first. Next, the heterogeneous system in its initial configuration subjected to the same loading and boundary conditions was solved. Then the boundary integrals in Eqs. (14), (15), or (17)

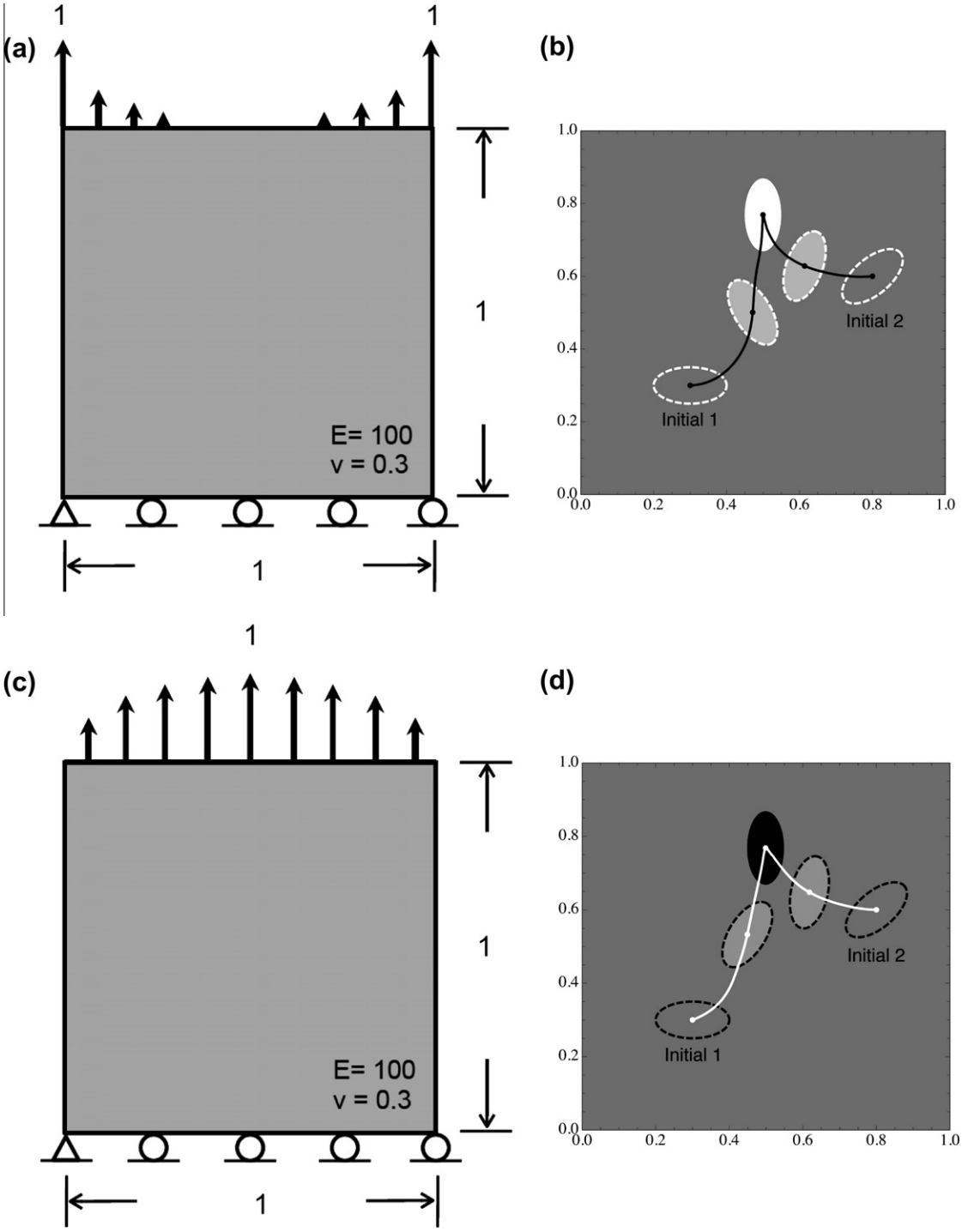

Fig. 4. Optimal configuration and the iterates resulting from two different initial configurations when both position as well as orientation are sequentially modified: (a) quadratically distributed traction for insertion of a single elliptical hole, (b) optimal configuration of the hole, (c) quadratically distributed traction for insertion of a single elliptical inclusion, and (d) optimal configuration of the inclusion ($E = 1000$).

were evaluated to obtain the sensitivity corresponding to translation, rotation or geometrical scaling of the feature, respectively. Once the configurational derivative was estimated, the configuration of the heterogeneity was updated using the descent/ascent directions corresponding to Eqs. (14)–(17). The above procedure was iterated until the optimality condition was satisfied. The flow of control during the analysis is shown in Fig. 3.

We show, in Appendix D, illustrative examples that demonstrate the convergence to optimal position, orientation and scale of a single elliptical, finite-sized feature. The examples proceed in a sequence starting with those that illustrate individually the optimal position of finite sized features (Eq. (14)), followed by optimal orientation (Eq. (15)), and scaling (Eq. (16) or Eq. (17)).

4. Demonstration examples

In the examples of the previous section, the position, orientation, and scale of a heterogeneity were individually optimized using the associated configurational derivative expressions. Here,

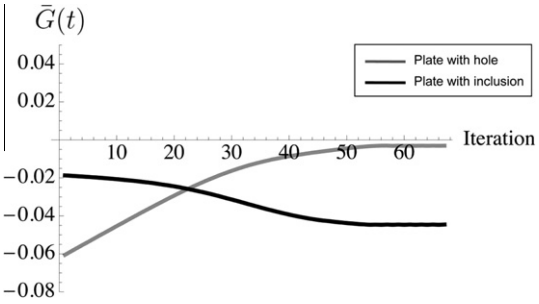

Fig. 5. Normalized objectives of plate with heterogeneities placed at position 1 in Fig. 4 against iteration count. The plotted quantities are normalized with respect to the total compliance of homogeneous plates subjected to quadratically distributed tractions.

we demonstrate the proposed methodology for optimal topological design by optimizing the configuration of finite-sized heterogeneities enabled by the derived configurational derivative.

4.1. Simultaneous optimization of position and orientation of an elliptical heterogeneity

In the first example, we iteratively update the location as well as the orientation of holes as well as inclusions of fixed shape and size in an alternating sequence until the optimal configuration is reached. The quadratically varying tractions illustrated in Fig. 4(a) and (c) were applied (the chosen load distributions were aimed at ensuring a unique solution for the single hole/inclusion problem), and two possible initial configurations were considered in each case. The optimal location and orientation of the heterogeneities that resulted from the iterations are shown in Fig. 4. To provide further insight into the intermediate iterations, we plot the change in the objective of the heterogeneous structures (corresponding to initial location 1) in Fig. 5. The objective of the heterogeneous plate decreases (increases) as the inclusion (hole) evolves towards the optimal configuration.

4.2. Simultaneous optimization of position and orientation of holes with regular shapes

Next, we illustrate the configurational optimization of holes with regular shapes (circular, elliptical, and stadium-shaped holes), which are commonly used in engineering practice. We used the structure shown in Fig. 4(a) as before to ensure a unique solution for each shape. The initial (arbitrarily chosen) and the corresponding optimal configurations of the above mentioned hole shapes that possessed an identical area are illustrated in Fig. 6(a) and (b). To enable a comparison with the classical topological derivative-derived solution, the location where condition Eq. (25) was

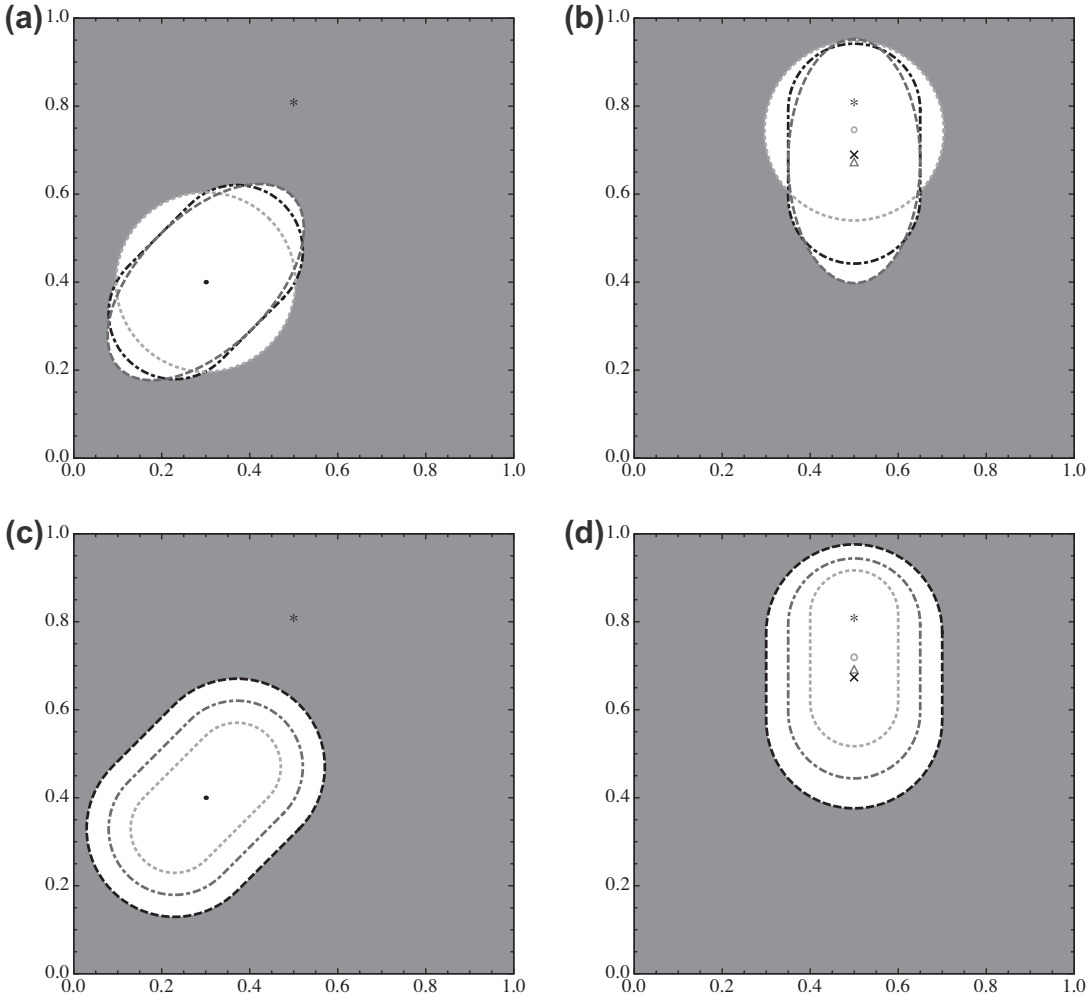

Fig. 6. Optimal configurations of regular holes of varying shape (area held same) and stadium holes of varying size: (a) initial configurations of circular, elliptical, and stadium-shaped holes, (b) optimal configurations, (c) initial configurations of three stadium-shaped holes with different sizes, and (d) optimal configurations of the considered hole sizes. The asterisks represent the optimal locations for inserting an infinitesimal hole based on Eq. (25).

satisfied is also marked (asterisk) in the figures to represent the optimal position for inserting an infinitesimal hole.

Further, the effect of hole size on the resulting optimal configuration was studied by considering three stadium holes with different sizes, as illustrated in Fig. 6(c) and (d). It was observed that the optimal location varies as a function of hole size. Thus, we conclude that the optimal position of an inserted hole depends on its shape and size. In addition, the centers of the optimally placed finite-sized holes are different from the optimal location for inserting an infinitesimal hole obtained using Eq. (25). The configurational derivative used here permits the size and shape of the hole be fixed to meet designer's intent or manufacturing constraint.

4.3. Topology optimization through insertion of heterogeneities

In the following examples, we demonstrate the methodology for topology optimization by sequentially inserting finite-sized heterogeneities in a homogeneous structure.

4.3.1. Optimization through sequential insertion of infinitesimal/finite-sized holes

In this example, we determine the optimal topology and shape by sequentially introducing holes into a structure and subsequently scaling them using Eq. (17). The overall philosophy adopted here can be viewed as a generalized "Bubble" method (Eschenauer et al., 1994) for finite-sized heterogeneities. Both sequential introduction of infinitesimal holes followed by their shape optimization, as in the Bubble method, and topological optimization through introduction of finite-sized holes are considered here.

We first consider a plate subjected to loading and boundary conditions shown in Fig. 7. In the first scenario, we sequentially inserted infinitesimal holes at the location where Eq. (25) was satisfied and the objective ψ^0 was a minimum. Due to the symmetry of load and geometry, two possible locations for the introduction of the holes were identified in the structure marked with an asterisk in Fig. 8(a). In order to preserve the symmetry of the optimized

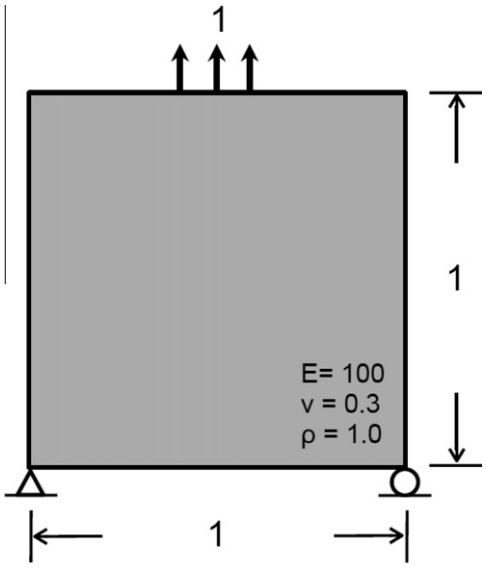

Fig. 7. Plate subjected to distributed load on top and the illustrated boundary conditions at the bottom used in the examples demonstrating sequential topological modification.

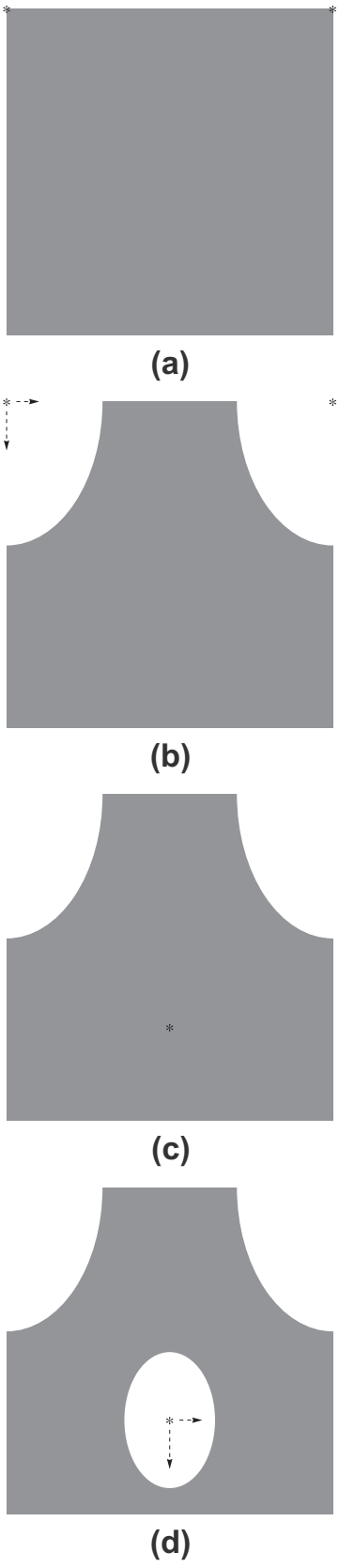

Fig. 8. Topology optimization through insertion of infinitesimal holes into structure of Fig. 7: (a) optimal hole locations identified during the first iteration, (b) optimal size of the first two holes, (c) optimal hole location identified during the second iteration, and (d) optimal size of the third hole.

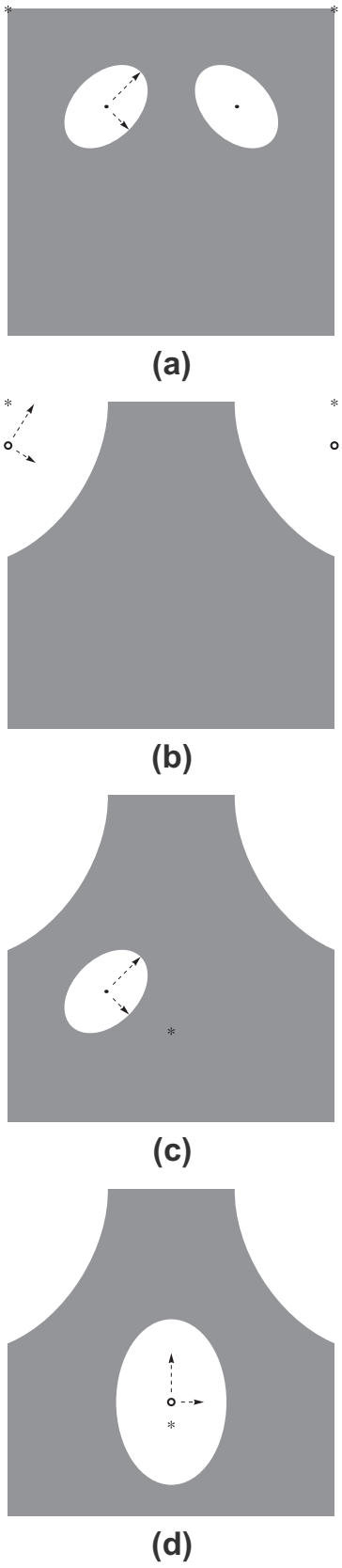

Fig. 9. Topology optimization through sequential insertion of finite-sized holes into the structure of Fig. 7: (a) initial configurations of the first two holes inserted during first iteration, (b) optimal configurations of the holes, (c) initial configuration of the third hole inserted during second iteration, and (d) optimal configuration of the hole.

structure, we introduced two elliptical primitives (representing the infinitesimal holes) with identical aspect ratio and orientation at these locations. The size of the holes were subsequently uniformly scaled to their optimum according to Eq. (17) using a chosen weight $\bar{w} = 0.4$, while the location and orientation were kept fixed. Since the holes were placed on the boundary, the topology optimization process led to a modification on the external shape of the plate as shown in Fig. 8(b). The above two steps were iteratively repeated to yield the topologically modified structure as illustrated in Fig. 8(c) and (d).

The alternative, second design approach involved directly inserting finite-sized holes, whose location, orientation, as well as scale were arbitrarily chosen initially and updated in accordance with the configurational derivative. We chose the same weight $\bar{w} = 0.4$ as before in determining the optimal size. A geometrical constraint was enforced to ensure that the center of a hole stayed within the square region of the plate (so structures with holes or modified boundaries were obtained). We first inserted two finite-sized holes (same aspect ratio as in the first scenario) symmetrically about the mid-plane in anticipation of symmetrical resulting structure as illustrated in Fig. 9(a). Then the location, orientation, and scaling of the holes were updated iteratively until the corresponding optimal conditions were met. The configurationally

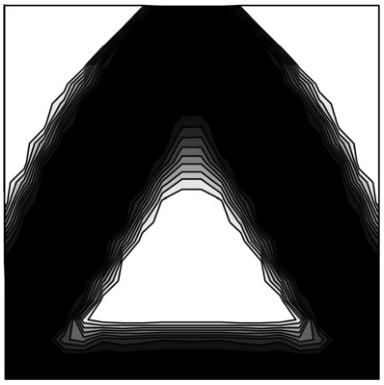

Fig. 10. Optimal topology obtained through material redistribution of structure shown in Fig. 7. $\bar{w}$ of 0.5 was used to obtain the solution (Rayasam et al., 2007a).

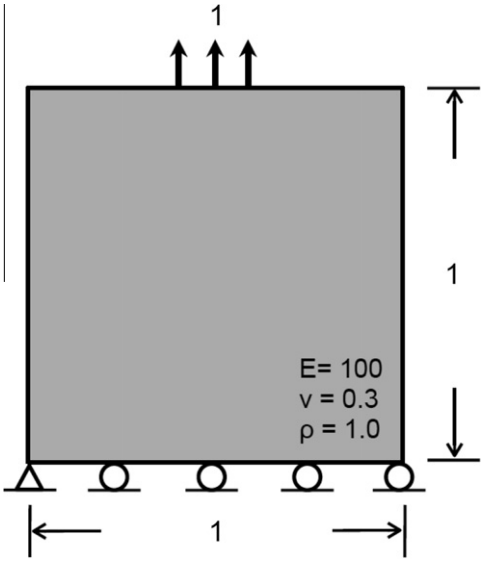

Fig. 11. A plate subjected to distributed load on top and boundary conditions as illustrated in the figure at the bottom.

optimized holes, which led to a modification on the external shape, are shown in Fig. 9(b). In the next step of topological design, we inserted a third hole and carried out configurational optimization. The initial and optimal configurations of the third hole are shown in Fig. 9(c) and (d).

It is observed from Fig. 9(b) and (d) that the location, orientation, as well as scaling of the optimal holes in the second approach are different from those obtained using the first approach. A similar A-frame like optimal structures corresponding to the same loading and boundary conditions was obtained in Rayasam et al. (2007a) through the classical topology optimization technique of material redistribution as illustrated in Fig. 10.

Next, we consider the same initial structure as before, but with boundary conditions as shown in Fig. 11. As before, both infinitesimal topological modification followed by shape optimization as well as finite-sized topological modification are carried out. For this problem, two additional locations where the (infinitesimal) condition of Eq. (25) was satisfied were observed (see Fig. 12(a)). Therefore, we introduced elliptical primitives at either of the pair

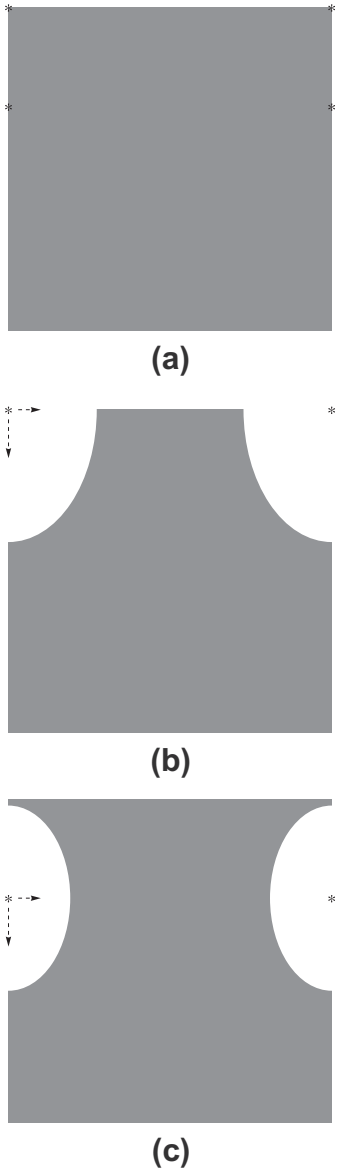

Fig. 12. Topology optimization through insertion of infinitesimal holes into structure of Fig. 11: (a) optimal hole locations identified, (b) optimal size of the two holes initially placed at the upper corners, and (c) optimal size of the two holes initially placed at the lower locations.

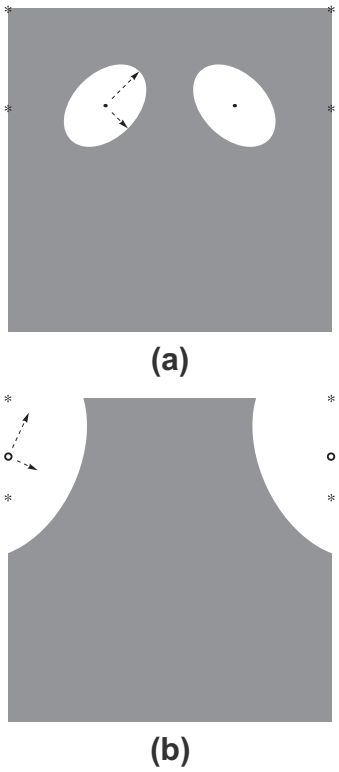

Fig. 13. Topological optimization through insertion of finite-sized holes into the structure of Fig. 11: (a) initial configurations of the arbitrarily inserted holes and (b) optimized configurations of the holes.

of symmetric locations thus identified, and then iteratively scaled them to their optimal sizes using a chosen weight $\bar{w} = 0.4$ (see Fig. 12(b) and (c)). In contrast, finite-sized elliptical holes were inserted with the initial configurations illustrated in Fig. 13(a) for finite-sized topological design. The holes were iteratively modified to their optimal configurations as shown in Fig. 13(b). This new boundary condition, however, eliminated the optimal location at the center of the plate identified during the second step of optimization with the earlier boundary condition (see Fig. 8(c)).

4.3.2. Topology optimization through insertion finite-sized inclusions

We next illustrate topological modification by insertion of finite-sized inclusions into the structure shown in Fig. 7. In this structure, the gradient of the energy density is non-zero at support and load locations, which are the local maxima of energy density. Since there was no location within the structure where Eq. (25) was satisfied, we arbitrarily placed two elliptical inclusions (with $E = 200$ and $\rho = 2$) at symmetric locations (see Fig. 14(a)). We then used the configurational derivative corresponding to translation, rotation, and uniform scaling to sequentially update the configurations of the inclusions at each iterate. The optimal configurations of the inclusions as well as the intermediate iterates are shown in Fig. 14(b)–(f).

5. Concluding remarks

In this paper, we posed a configuration optimization problem and subsequently derived the configurational derivative that describes the effect of moving stiff or soft inclusion boundaries placed inside a domain with moving boundaries. The configurational derivative was shown to extend the topological derivative to finite-sized inclusions and to simplify to shape design sensitivity when it is computed independent of the homogeneous domain. The developed derivative together with the isogeometric

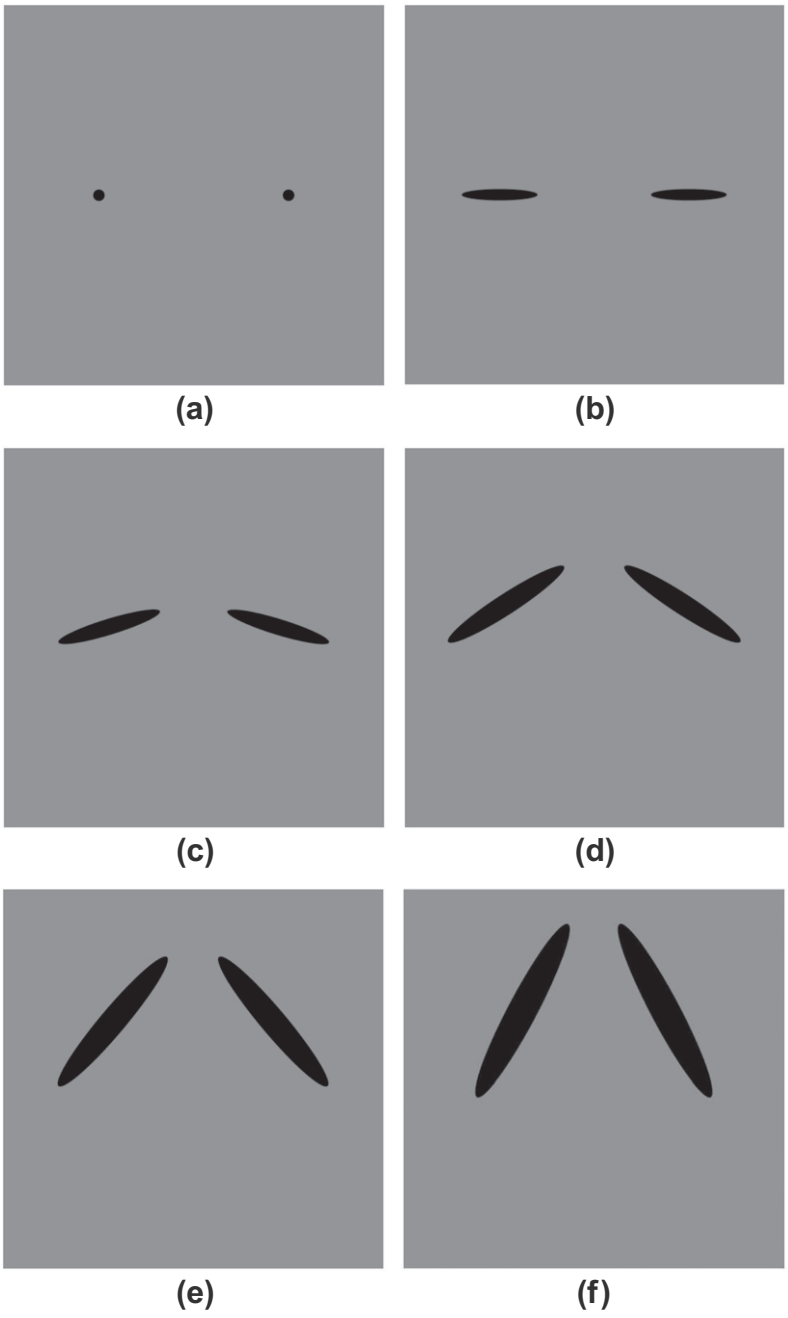

Fig. 14. Topology optimization through insertion of finite-sized inclusions into the plate of Fig. 7: (a) initial locations where the finite-sized inclusions were inserted; (b)–(e) Intermediate iterates; and (f) optimal configuration of the inclusions corresponding to $\bar{w} = 0.4$.

procedure for topological optimization through material redistribution demonstrated earlier (see Fig. 10 from Rayasam et al. (2007a)) enables the developed procedure to seamlessly unify the three possible approaches to topological modifications, namely through material redistribution, through sequential or simultaneous introduction of finite-sized (or infinitesimal) inclusions or holes, and finally through heterogeneity merging and separation.

Acknowledgments

Former doctoral students M. Rayasam and K. Mysore contributed to preliminary numerical experiments that provided the motivation for the present paper.

Appendix A. Derivation of configurational derivative

The Lagrangian $G(t)$ is identical to $g(t)$ if the constraints in Problem (4) are satisfied at every instant. Also, in the Lagrangian, since the virtual displacements are arbitrary, the Lagrange multiplier corresponding the overall virtual work constraint are absorbed into the virtual displacements. Now, considering the right hand side, the material derivative of the first term $\frac{D}{Dt}\int_\Omega \psi d\Omega$ over the heterogeneous domain is derived below. By using the material derivative operator $(\frac{D}{Dt} = \frac{\partial}{\partial t} + \mathbf{v}\cdot\nabla)$ and the fact that $d\Omega = Jd\Omega^{t_0}$ with J being the Jacobian of the deformation $\mathbf{x}$, the material derivative of the functional $f(t)$ may be derived as follows Malvern, 1969:

$$\begin{aligned}\dot{f}(t) &= \int_\Omega \dot{\psi}\, d\Omega + \int_\Omega \psi \frac{\dot{J}}{J} d\Omega \\ &= \int_\Omega \left(\frac{\partial \psi}{\partial t} + \mathbf{v}\cdot\nabla\psi\right) d\Omega + \int_\Omega \psi \nabla\cdot\mathbf{v}\, d\Omega \\ &= \int_\Omega \frac{\partial \psi}{\partial t}\, d\Omega + \int_\Omega \nabla\cdot(\psi\mathbf{v})\, d\Omega \\ &= \int_\Omega \frac{\partial \psi}{\partial t}\, d\Omega + \int_\Gamma \psi v_n d\Gamma + \int_{\Gamma_p} [[\psi v_n]] d\Gamma \end{aligned} \tag{26}$$

where $\dot{J} = J\nabla\cdot\mathbf{v}$ (see Malvern, 1969) was used to arrive at the second step, v_n is the normal component of design velocity, i.e., $v_n = \mathbf{v}\cdot\mathbf{n}$ and $[[\cdot]]$ denotes the jump in value across the inclusion boundary defined as $[[a]] = a^+ + a^-$ with the superscripts $+$ and $-$ denoting the value of the quantity on either side of the boundary. The existence of the jump term depends on the particular choice of the design function ψ and its continuity across the inclusion interface.

Similarly, the material derivative of the second group of terms in Eq. (5) is obtained by employing (in addition to $\dot{J} = J\nabla\cdot\mathbf{v}$) the material derivative of Nanson's formula (Malvern, 1969) $d\dot{\Gamma} = [\nabla\cdot\mathbf{v} - \mathbf{n}\cdot\nabla\mathbf{v}\cdot\mathbf{n}]d\Gamma$:

$$\begin{aligned}&\frac{D}{Dt}\left(\int_\Omega \varepsilon : \mathbf{C} : \varepsilon^a d\Omega - \int_\Gamma \mathbf{t}\cdot\mathbf{u}^a d\Gamma\right) = \int_\Omega \dot{\varepsilon} : \mathbf{C} \\ &: \varepsilon^a d\Omega + \left(\int_\Omega \varepsilon : \mathbf{C} : \dot{\varepsilon}^a d\Omega - \int_\Gamma \mathbf{t}\cdot\dot{\mathbf{u}}^a d\Gamma\right) \\ &+ \left(\int_\Omega \varepsilon : \mathbf{C} : \varepsilon^a(\nabla\cdot\mathbf{v}) d\Omega - \int_\Gamma (\mathbf{t}\cdot\mathbf{u}^a)[\nabla\cdot\mathbf{v} - \mathbf{n}\cdot\nabla\mathbf{v}\cdot\mathbf{n}] d\Gamma\right)\end{aligned} \tag{27}$$

where, it has been assumed that the tractions and displacements are continuous across the inclusion boundary. If we assume further that $\dot{\varepsilon}^a$ and $\dot{\mathbf{u}}^a$ are also compatible, then the second group on the right hand side vanishes. Since, in the absence of spontaneous change of $\mathbf{u}^a, \dot{\mathbf{u}}^a = \mathbf{v}\cdot\nabla\mathbf{u}^a$ and since $\nabla\mathbf{u}^a$ is in general not zero on Γ_u, for $\dot{\mathbf{u}}^a$ to serve as arbitrary virtual "displacements" that vanish on Γ_u, it is necessary that $\mathbf{v} = 0$ on Γ_u.

Denoting $L(t) = \int_\Omega \psi d\Omega - \left(\int_\Omega \varepsilon : \mathbf{C} : \varepsilon^a d\Omega - \int_\Gamma \mathbf{t}\cdot\mathbf{u}^a d\Gamma\right)$, we obtain the material derivative of $L(t)$ by combining Eqs. (26) and (27):

$$\begin{aligned}\dot{L}(t) = &\int_\Omega \frac{\partial \psi}{\partial t} d\Omega + \int_\Gamma \psi v_n + \int_{\Gamma_p} [[\psi v_n]] d\Gamma - \int_\Omega \dot{\varepsilon} : \mathbf{C} : \varepsilon^a d\Omega \\ &- \int_\Omega (\varepsilon : \mathbf{C} : \varepsilon^a)(\nabla\cdot\mathbf{v}) d\Omega + \int_{\Gamma_t} (\mathbf{t}\cdot\mathbf{u}^a)[\nabla\cdot\mathbf{v} - \mathbf{n}\cdot\nabla\mathbf{v}\cdot\mathbf{n}] d\Gamma\end{aligned} \tag{28}$$

where we have used the fact that $\mathbf{u}^a$ as well as $\mathbf{v}$ vanish on Γ_u. We now define an adjoint traction vector and rewrite the above equation using the definition of v_n, and the relation (ignoring spontaneous change in $\mathbf{u}$) $\dot{\mathbf{u}} = \mathbf{v}\cdot\nabla\mathbf{u}$:

$$\begin{aligned}\dot{L}(t) = &\int_\Omega \frac{\partial \psi}{\partial t} d\Omega + \int_{\Gamma_p} [[\psi v_n]] d\Gamma - \int_\Omega (\varepsilon : \mathbf{C} : \varepsilon^a)(\nabla\cdot\mathbf{v})\, d\Omega \\ &- \int_\Omega \dot{\varepsilon} : \mathbf{C} : \varepsilon^a\, d\Omega + \int_\Gamma \mathbf{t}^a\cdot\dot{\mathbf{u}}\, d\Gamma + \int_{\Gamma_t} (\psi\mathbf{n} - \mathbf{t}^a\cdot\nabla\mathbf{u}^T)\cdot\mathbf{v}\, d\Gamma \\ &+ \int_{\Gamma_t} (\mathbf{t}\cdot\mathbf{u}^a)[\nabla\cdot\mathbf{v} - \mathbf{n}\cdot\nabla\mathbf{v}\cdot\mathbf{n}] d\Gamma\end{aligned} \tag{29}$$

where we have used $\mathbf{v} = 0$ on Γ_u. The above expression can be further simplified by defining an adjoint boundary value problem for the solution of the adjoint quantities:

$$\int_\Omega \dot{\varepsilon} : \mathbf{C} : \varepsilon^a\, d\Omega - \int_\Gamma \mathbf{t}^a\cdot\dot{\mathbf{u}}\, d\Gamma = 0 \tag{30}$$

where exploiting the symmetry of $\mathbf{C}$, $\dot{\varepsilon}$ may be considered as the virtual strain compatible with $\dot{\mathbf{u}}$ corresponding to the adjoint problem. Since $\mathbf{v}$ is an arbitrary velocity on Γ_t, the applied tractions corresponding to the adjoint boundary value problem are chosen to satisfy the following equation:

$$\mathbf{t}^a\cdot\nabla\mathbf{u}^T = \psi\mathbf{n} \text{ or equivalently } \mathbf{t}^a\cdot\nabla\mathbf{u}^T\cdot\mathbf{n} = \psi \text{ on } \Gamma_t \tag{31}$$

Although, the form of ψ is not restricted in the present derivation, it is convenient to seek ψ in the form $\psi = \mathbf{s} : \varepsilon$, where $\mathbf{s}$ is an arbitrary symmetric second order tensor. Then, since the scalar product of $\mathbf{s}$ with an antisymmetric tensor vanishes (i.e., since ε is the symmetric part of $\nabla\mathbf{u}^T$, $\psi = \mathbf{s} : \varepsilon = \mathbf{s} : \nabla\mathbf{u}^T$), we can obtain the adjoint traction vector as:

$$\begin{aligned}&\mathbf{t}^a\cdot\nabla\mathbf{u}^T\cdot\mathbf{n} = \psi \text{ on } \Gamma_t \Rightarrow (\mathbf{t}^a\mathbf{n}) : \nabla\mathbf{u}^T - \psi = 0 \\ &(\mathbf{t}^a\mathbf{n} - \mathbf{s}) : \nabla\mathbf{u}^T = 0 \Rightarrow \mathbf{t}^a = \mathbf{s}\cdot\mathbf{n} \text{ on } \Gamma_t\end{aligned} \tag{32}$$

Substituting Eqs. (30) and (31), Eq. (29) can be reduced to:

$$\begin{aligned}\dot{L}(t) = &\int_\Omega \frac{\partial \psi}{\partial t} d\Omega + \int_{\Gamma_p} [[\psi v_n]] d\Gamma - \int_\Omega (\varepsilon : \mathbf{C} : \varepsilon^a)(\nabla\cdot\mathbf{v})\, d\Omega \\ &+ \int_{\Gamma_t} (\mathbf{t}\cdot\mathbf{u}^a)[\nabla\cdot\mathbf{v} - \mathbf{n}\cdot\nabla\mathbf{v}\cdot\mathbf{n}] d\Gamma\end{aligned} \tag{33}$$

Repeating the above process for the homogeneous body to derive $\dot{L}^0(t)$ with its corresponding adjoint boundary value problem, and following the steps used in Eq. (26) for the mass term in $G(t)$, we arrive at the material derivative of the desired quantity $G(t)$ (defined in Eq. (5)) as:

$$\begin{aligned}\dot{G}(t) = &\int_\Omega \frac{\partial}{\partial t}(\psi - \psi^0) d\Omega + w\int_{\Omega_p} \frac{\partial}{\partial t}(\rho - \rho^0) d\Omega \\ &+ \int_{\Gamma_p} [[(\psi + w\rho) v_n]] d\Gamma \\ &- \int_\Omega \left(\varepsilon : \mathbf{C} : \varepsilon^a - \varepsilon^0 : \mathbf{C}^0 : \varepsilon^{a0}\right)(\nabla\cdot\mathbf{v})\, d\Omega \\ &+ \int_{\Gamma_t} \left(\mathbf{t}\cdot\mathbf{u}^a - \mathbf{t}^0\cdot\mathbf{u}^{a0}\right)[\nabla\cdot\mathbf{v} - \mathbf{n}\cdot\nabla\mathbf{v}\cdot\mathbf{n}] d\Gamma\end{aligned} \tag{34}$$

Rearrangement of terms in the above equation leads to Eq. (6).

Appendix B. Derivation of alternative form of sensitivity to scaling

We begin by rewriting the last integral in Eq. (16) as:

$$\int_{\Gamma_t} \mathbf{t}\cdot(\mathbf{u}^a - \mathbf{u}^{a0}) d\Gamma = \int_\Gamma \mathbf{t}\cdot\tilde{\mathbf{u}}^a d\Gamma = \int_\Omega \varepsilon : \mathbf{C} : \tilde{\varepsilon}^a d\Omega \tag{35}$$

where, $\tilde{\mathbf{u}}^a$ and $\tilde{\varepsilon}^a$ are defined as $\tilde{\mathbf{u}}^a = \mathbf{u}^a - \mathbf{u}^{a0}$ and $\tilde{\varepsilon}^a = \varepsilon^a - \varepsilon^{a0}$, and we have treated $\tilde{\varepsilon}^a$ as the virtual strain compatible with the virtual displacement $\tilde{\mathbf{u}}^a$ on the heterogeneous body. We have also applied the divergence theorem in a standard manner (using the fact that stresses satisfy equilibrium equations) to arrive at the domain integral. Thus, we can rewrite the above equation as:

$$\begin{aligned}\int_\Gamma \mathbf{t}\cdot\tilde{\mathbf{u}}^a\, d\Gamma = \int_\Omega \varepsilon : \mathbf{C} : \tilde{\varepsilon}^a d\Omega = &\int_{\Omega_p^+} \varepsilon : \mathbf{C} : \tilde{\varepsilon}^a d\Omega + \\ &\int_{\Omega - \Omega_p^+} \varepsilon : \mathbf{C} : \tilde{\varepsilon}^a d\Omega = \int_{\Omega_p^+} \varepsilon : \mathbf{C} : \tilde{\varepsilon}^a d\Omega + \int_{\Omega - \Omega_p^+} \tilde{\varepsilon}^a : \mathbf{C} : \varepsilon d\Omega\end{aligned} \tag{36}$$

where we have used the symmetry property of $\mathbf{C}$ in the last step. Now, applying the divergence theorem together with the fact that original and adjoint stresses satisfy equilibrium, we get:

$$\int_\Gamma \mathbf{t}\cdot\tilde{\mathbf{u}}^a\,d\Gamma = \int_{\Gamma_p^+}\mathbf{t}\cdot\tilde{\mathbf{u}}^a\,d\Gamma + \left(\int_\Gamma \tilde{\mathbf{t}}^a\cdot\mathbf{u}\,d\Gamma - \int_{\Gamma_p^+}\tilde{\mathbf{t}}^a\cdot\mathbf{u}\,d\Gamma\right)$$
$$= \int_{\Gamma_p^+}(\mathbf{t}\cdot\tilde{\mathbf{u}}^a - \tilde{\mathbf{t}}^a\cdot\mathbf{u})d\Gamma + \int_\Gamma \tilde{\mathbf{t}}^a\cdot\mathbf{u}\,d\Gamma$$
$$= \int_{\Gamma_p^+}(\mathbf{t}^{a0}\cdot\mathbf{u} - \mathbf{t}\cdot\mathbf{u}^{a0})d\Gamma + \int_\Gamma(\mathbf{t}^a - \mathbf{t}^{a0})\cdot\mathbf{u}\,d\Gamma \tag{37}$$

where $\tilde{\mathbf{t}}^a = (\mathbf{t}^a - \mathbf{t}^{a0})$, the negative sign for the last integral relative to the first integral in the first step is because of the reversal of sign of the normal and we have used the symmetry property of $\mathbf{C}$ resulting in the reciprocal property on the heterogeneous domain: $\int_{\Gamma_p^+}\mathbf{t}^a\cdot\mathbf{u}d\Gamma = \int_{\Gamma_p^+}\mathbf{t}\cdot\mathbf{u}^a d\Gamma$. In the above derivation, one needs to keep in mind that on Γ_p^+, $\tilde{\mathbf{t}}^a/\tilde{\mathbf{u}}^a$ is the difference between adjoint tractions/displacements applied on two *different* bodies respectively.

Finally, substituting the above expression into Eq. (16), we obtain the sensitivity to scaling as given in Eq. (17).

Appendix C. Derivation for jump in objective ψ on a spherical surface

We consider an inclusion under the influence of a macrostrain ε^0. We first derive below the expression for the jump in objective ψ on the boundary Γ_p in terms of the elasticity tensors as well as the applied strain field ε^0. To do so, we begin with the well established approach of micromechanics (Nemat-Nasser and Hori, 1999) by introducing an eigenstrain ε^* to describe an *equivalent homogeneous* solid with matrix material behavior such that:

$$\sigma^+ = \mathbf{C}^0 : \varepsilon^+(\mathbf{x}) \tag{38}$$
$$\sigma^- = \mathbf{C}^0 : (\varepsilon^-(\mathbf{x}) - \varepsilon^*(\mathbf{x})) \tag{39}$$

where $(\cdot)^-/(\cdot)^+$ refer to quantities just inside/outside the inclusion boundary Γ_p respectively. The consistency condition (between the heterogeneous and equivalent homogeneous descriptions) for the stress in the inclusion yields the relation:

$$\begin{aligned}&\sigma^-(\mathbf{x}) = \mathbf{C}:\varepsilon^-(\mathbf{x}) = \mathbf{C}^0:(\varepsilon^-(\mathbf{x}) - \varepsilon^*(\mathbf{x}))\\ &\text{or, } \left(\mathbf{C}-\mathbf{C}^0\right):\varepsilon^-(\mathbf{x}) = -\mathbf{C}^0:\varepsilon^*(\mathbf{x})\end{aligned} \tag{40}$$

The matrix as well as the inclusion are assumed isotropic with the elasticity tensors expressed as:

$$\mathbf{C}^0_{ijkl} = \lambda^0\delta_{ij}\delta_{kl} + \mu^0(\delta_{ik}\delta_{jl} + \delta_{il}\delta_{jk}) \tag{41}$$
$$\mathbf{C}_{ijkl} = \lambda\delta_{ij}\delta_{kl} + \mu(\delta_{ik}\delta_{jl} + \delta_{il}\delta_{jk}) \tag{42}$$

where $\lambda^0, \mu^0, \lambda$, and μ are Lamé constants corresponding to the matrix and the inclusion respectively. The eigenstrain within a spherical inclusion is a constant times that of the applied field given by Nemat-Nasser and Hori (1999)

$$\varepsilon^* = -(\mathbf{A}+\mathbf{S})^{-1}:\varepsilon^0 \tag{43}$$

where $\mathbf{A} = \left(\mathbf{C}-\mathbf{C}^0\right)^{-1}:\mathbf{C}^0$ and $\mathbf{S}$ is the fourth rank Eshelby tensor defined for a spherical inclusion as (Nemat-Nasser and Hori, 1999):

$$\mathbf{S}_{ijkl} = \frac{(3\lambda^0 - 2\mu^0)}{15(\lambda^0+2\mu^0)}\delta_{ij}\delta_{kl} + \frac{(3\lambda^0+8\mu^0)}{15(\lambda^0+2\mu^0)}(\delta_{ik}\delta_{jl}+\delta_{il}\delta_{jk}) \tag{44}$$

While, in general, $\mathbf{S}$ does not possess major symmetry, the above special case for an isotropic spherical inclusion does possess such a symmetry. Using Eqs. (40) and (43), the strain inside the inclusion can be expressed as:

$$\varepsilon^-(\mathbf{x}) = -\left(\mathbf{C}-\mathbf{C}^0\right)^{-1}:\mathbf{C}^0:\varepsilon^*(\mathbf{x}) = \mathbf{A}:(\mathbf{A}+\mathbf{S})^{-1}:\varepsilon^0 \tag{45}$$

Now, on Γ_p, we require displacement and traction compatibility, that is

$$\mathbf{u}^- = \mathbf{u}^+ \tag{46}$$
$$-\mathbf{n}^+\cdot\sigma^+ = \mathbf{n}\cdot\sigma^+ = \mathbf{n}^-\cdot\sigma^- \tag{47}$$

where $\mathbf{n} = \mathbf{n}^- = -\mathbf{n}^+$ is the outward normal to the inclusion boundary. Thus, using Eq. (39), we can rewrite the traction compatibility condition as:

$$\mathbf{n}\cdot\mathbf{C}^0:(\varepsilon^+ - \varepsilon^-) = -\mathbf{n}\cdot\sigma^* \text{ on } \Gamma_p \tag{48}$$

where $\sigma^* = \mathbf{C}^0:\varepsilon^*$.

The gradients of displacements are in general not compatible and we define the jump in the gradient of the displacements normal to the interface Γ_p as follows:

$$(\nabla\mathbf{u}^+ - \nabla\mathbf{u}^-)\cdot\mathbf{n} = \boldsymbol{\beta} \text{ on } \Gamma_p \tag{49}$$

Using the strain–displacement relation $\varepsilon = \frac{\nabla\mathbf{u}+\nabla\mathbf{u}^T}{2}$ as well as the fact that the product of a symmetric and anti-symmetric tensor is zero, the above expression can be rewritten as:

$$\mathbf{C}^0:(\varepsilon^+ - \varepsilon^-) = \mathbf{C}^0:\boldsymbol{\beta}\mathbf{n} \text{ on } \Gamma_p \tag{50}$$

Alternatively, using Eq. (38), the above equation may be expressed as:

$$\sigma^+ = \mathbf{C}^0:(\varepsilon^- + \boldsymbol{\beta}\mathbf{n}) \tag{51}$$

Substituting Eq. (50) into the traction compatibility condition of Eq. (48) we can derive and expression for $\mathbf{n}\boldsymbol{\beta}$ as:

$$\mathbf{n}\boldsymbol{\beta} = -\mathbf{D}^0:\sigma^* \tag{52}$$

where $\mathbf{D}^0 = \mathbf{n}\left(\mathbf{n}\cdot\mathbf{C}^0\cdot\mathbf{n}\right)^{-1}\mathbf{n}$, with the property $\mathbf{D}^0:\mathbf{C}^0:\mathbf{D}^0 = \mathbf{D}^0$. The expression for the fourth rank tensor $\mathbf{D}^0$ may be written explicitly as:

$$\mathbf{D}^0_{ijkl} = -\frac{(\lambda^0+\mu^0)}{\mu^0(\lambda^0+2\mu^0)}n_in_jn_kn_l + \frac{1}{\mu^0}n_i\delta_{jk}n_l \tag{53}$$

It is important to observe that the above tensor does not have symmetry with respect to i and j components, or with respect to k and l components, and it does not have symmetry between ij and kl components.

Finally, using Eqs. (45), (51) and (52), and exploiting the major and minor symmetries of the fourth rank tensor $\mathbf{C}^0$ as well as the symmetry of the tensor σ^*, we can derive the expression for the jump in the objective as:

$$\begin{aligned}\psi^+ - \psi^- = \sigma^+:\varepsilon^+ - \sigma^-:\varepsilon^- &= (\boldsymbol{\beta}\mathbf{n}):\mathbf{C}^0:(\boldsymbol{\beta}\mathbf{n}) + \varepsilon^-:\mathbf{C}^0:(\boldsymbol{\beta}\mathbf{n}) + (\boldsymbol{\beta}\mathbf{n})\\ &:\mathbf{C}^0:\varepsilon^- - \varepsilon^-:\left(\mathbf{C}-\mathbf{C}^0\right):\varepsilon^- = \sigma^*\\ &:\left[\mathbf{D}^0 + \left(\mathbf{C}-\mathbf{C}^0\right)^{-1}:\mathbf{C}^0:\mathbf{D}^0 + \mathbf{D}^0:\mathbf{C}^0:\left(\mathbf{C}-\mathbf{C}^0\right)^{-1} - \left(\mathbf{C}-\mathbf{C}^0\right)^{-1}\right]\\ &:\sigma^* = \sigma^*:\mathbf{B}:\sigma^*\end{aligned} \tag{54}$$

where $\mathbf{B}$ is a fourth rank tensor. Using Eq. (43), we can express the constant stress σ^* in terms of the macrostrain ε^0 as:

$$\sigma^*_{ij} = \left[a_1\delta_{ij}\delta_{kl} + a_2(\delta_{ik}\delta_{jl}+\delta_{il}\delta_{jk})\right]\varepsilon^0_{kl} \tag{55}$$

where, the coefficients a_1 and a_2 are:

$$\begin{aligned}a_1 = &\frac{3(\lambda^0+2\mu^0)}{(3\lambda+2\mu+4\mu^0)\left[2\mu^0(8\mu+7\mu^0)+\lambda^0(6\mu+9\mu^0)\right]}\\ &\times\Big\{-4(\mu-\mu^0)^2\mu^0 + \lambda^{0^2}(6\mu+9\mu^0)\\ &+\lambda^0(-4\mu^2+14\mu\mu^0+20\mu^{0^2})\\ &-3\lambda\left[\lambda^0(2\mu+3\mu^0)+2\mu^0(\mu+4\mu^0)\right]\Big\}\end{aligned} \tag{56}$$

$$a_2 = -\frac{15(\mu-\mu^0)\mu^0(\lambda^0+2\mu^0)}{2\mu^0(8\mu+7\mu^0)+\lambda^0(6\mu+9\mu^0)} \tag{57}$$

We note that Eq. (54) can be further simplified by using the explicit expression for the fourth rank tensor $\mathbf{D}^0$, which results in the following form for the tensor $\mathbf{B}$:

$$\begin{aligned}\mathbf{B}_{ijkl} = {} & b_1\delta_{ij}\delta_{kl} + b_2(\delta_{ik}\delta_{jl}+\delta_{il}\delta_{jk}) + b_3\delta_{ij}n_kn_l + b_4n_in_j\delta_{kl} \\ & + b_5\delta_{ik}n_jn_l + b_6n_in_k\delta_{jl} + b_7n_i\delta_{jk}n_l + b_8n_in_jn_kn_l\end{aligned} \tag{58}$$

with the coefficients $b_1 - b_8$ defined as:

$$b_1 = \frac{(\lambda-\lambda^0)}{2\left[3(\lambda-\lambda^0)+2(\mu-\mu^0)\right](\mu-\mu^0)} \tag{59}$$

$$b_2 = -\frac{1}{4(\mu-\mu^0)} \tag{60}$$

$$b_3 = b_4 = \frac{(\lambda^0\mu-\lambda\mu^0)}{(\mu-\mu^0)(\lambda^0+2\mu^0)\left[3(\lambda-\lambda^0)+2(\mu-\mu^0)\right]} \tag{61}$$

$$b_5 = b_6 = \frac{1}{2(\mu-\mu^0)} \tag{62}$$

$$b_7 = \frac{\mu}{\mu^0(\mu-\mu^0)} \tag{63}$$

$$b_8 = -\frac{(\lambda^0+\mu^0)(\mu+\mu^0)}{\mu^0(\mu-\mu^0)(\lambda^0+2\mu^0)} \tag{64}$$

Now, considering the integral $\int_{\Gamma_p}(\psi^- - \psi^+)\,d\Gamma_p = -\int_{\Gamma_p}\sigma^* : \mathbf{B} : \sigma^* d\Gamma_p$, since σ^* is constant, on a spherical surface with the normal defined by the vector $\mathbf{n} = [\sin(\theta)\cos(\phi), \sin(\theta)\sin(\phi), \cos(\theta)]^T$, the following results are of relevance in evaluating the integral:

$$\int_0^{\pi}\int_0^{2\pi} n_in_j(R\sin(\theta)d\phi)(Rd\theta) = \frac{4\pi R^2}{3}\delta_{ij} \tag{65}$$

$$\begin{aligned}&\int_0^{\pi}\int_0^{2\pi} n_in_jn_kn_l(R\sin(\theta)d\phi)(Rd\theta) \\ &= \frac{4\pi R^2}{15}\left[\delta_{ij}\delta_{kl} + (\delta_{ik}\delta_{jl}+\delta_{il}\delta_{jk})\right]\end{aligned} \tag{66}$$

Carrying out the integration and using Eq. (55), we can express the integral of the jump in compliance over the spherical surface as:

$$\int_{\Gamma_p}(\psi^- - \psi^+)d\Gamma_p = -\int_{\Gamma_p}\sigma^* : \mathbf{B} : \sigma^* d\Gamma_p = -\left(\varepsilon^0 : \hat{\mathbf{C}} : \varepsilon^0\right)\Gamma_p \tag{67}$$

where $\Gamma_p = 4\pi R^2$ and $\hat{\mathbf{C}}$ is a fourth rank isotropic tensor of the form:

$$\hat{\mathbf{C}}_{ijkl} = c_1\delta_{ij}\delta_{kl} + c_2(\delta_{ik}\delta_{jl}+\delta_{il}\delta_{jk}) \tag{68}$$

with the coefficients defined as:

$$\begin{aligned}c_1 = {} & \frac{3(\lambda^0+2\mu^0)}{(3\lambda+2\mu+4\mu^0)^2\left[2\mu^0(8\mu+7\mu^0)+\lambda^0(6\mu+9\mu^0)\right]^2} \\ & \times\left\{(3\lambda+2\mu+4\mu^0)\left[\lambda^0(6\mu-9\mu^0)+2(8\mu-7\mu^0)\mu^0\right]\right. \\ & \times\left[2\lambda^0\mu(3\lambda-3\lambda^0+2\mu)+\left(9\lambda\lambda^0-9\lambda^{0^2}+6\lambda\mu-14\lambda^0\mu+4\mu^2\right)\mu^0\right. \\ & \left.+4(6\lambda-5\lambda^0-2\mu)\mu^{0^2}+4\mu^{0^3}\right] \\ & -20(\mu-\mu^0)\mu^{0^2}(3\lambda+2\mu+4\mu^0)\left[2\mu(\lambda^0+6\mu^0)\right. \\ & \left.-\lambda(9\lambda^0+14\mu^0)\right]+6\mu^0\left[2\mu(\lambda^0+6\mu^0)-\lambda(9\lambda^0+14\mu^0)\right] \\ & \times\left[-4(\mu-\mu^0)^2\mu^0+\lambda^{0^2}(6\mu+9\mu^0)\right. \\ & +\lambda^0\left(-4\mu^2+14\mu\mu^0+20\mu^{0^2}\right) \\ & \left.\left.-3\lambda\left[\lambda^0(2\mu+3\mu^0)+2\mu^0(\mu+4\mu^0)\right]\right]\right\}\end{aligned} \tag{69}$$

$$c_2 = \frac{15(\mu-\mu^0)\mu^0(\lambda^0+2\mu^0)\left[\lambda^0(6\mu-9\mu^0)+2(8\mu-7\mu^0)\mu^0\right]}{\left[2\mu^0(8\mu+7\mu^0)+\lambda^0(6\mu+9\mu^0)\right]^2} \tag{70}$$

We evaluate the above expressions under two special conditions:

1. The trivial condition corresponding to $\lambda = \lambda^0$ and $\mu = \mu^0$, leading to $c_1 = c_2 = 0$.
2. Defining a fourth rank tensor $\mathbf{P} = \mathbf{C}^{0^{-1}} : \hat{\mathbf{C}}$ such that $\int_{\Gamma_p}(\psi^- - \psi^+)\,d\Gamma_p = -\left(\sigma^0 : \mathbf{P} : \varepsilon^0\right)\Gamma_p$, substituting $\lambda^0 = \frac{E^0\nu^0}{(1+\nu^0)(1-2\nu^0)}$, $\mu^0 = \frac{E^0}{2(1+\nu^0)}$ (and correspondingly for λ and μ), and setting the inclusion elastic modulus $E = 0$, we derive the expression for the tensor $\mathbf{P}$ for the case of a spherical hole as:

$$\mathbf{P}_{ijkl} = \frac{3}{2}\frac{(1-\nu^0)}{(7-5\nu^0)}\left[-\frac{(1-5\nu^0)}{(1-2\nu^0)}\delta_{ij}\delta_{kl} + 5\left(\delta_{ik}\delta_{jl}+\delta_{il}\delta_{jk}\right)\right] \tag{71}$$

$\mathbf{P}$ is the fourth rank *polarization tensor* (see Nazarov and Sokolowski, 2003; Ammari and Kang, 2005; Amstutz, 2006; Kang and Kim, 2007) corresponding to the introduction of a spherical inclusion. The specific form corresponding to the introduction of a spherical hole was also derived by Novotny et al. (2007) without using the notion of the polarization tensor. It should be noted here that the expression derived by Novotny et al. (2007) differs by a factor of $\frac{1}{2}$ from the above expression since the chosen objectives in the present work and in the referenced paper differ by a factor of $\frac{1}{2}$.

Appendix D. Examples illustrating convergence of single hole/inclusion

D.1. Optimal location of a heterogeneity

We begin with an example in which we attempted to determine the optimal location of an elliptical hole or inclusion inserted into a square plate. The plate geometry, loading and boundary conditions for hole and inclusion are shown in Figs. 15(a) and 16(a) respectively. We used quadratically distributed tractions to ensure a unique solution in these examples. Following the steepest descent direction corresponding to Eq. (14), the optimal locations for an elliptical hole and an elliptical inclusion of an identical size were obtained (see Figs. 15(b) and 16(b)). In both examples, the magnitude of the configurational derivative converged to zero regardless of the choice of initial location.

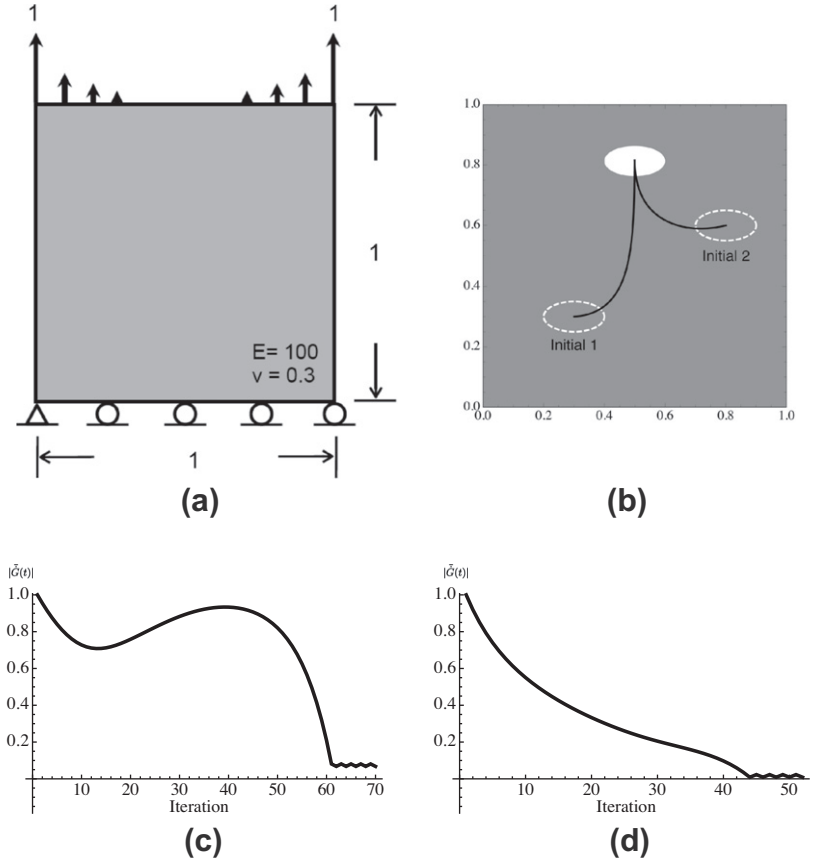

Fig. 15. Optimal location for inserting an elliptical hole in a square plate: (a) quadratically distributed traction, (b) iterates of holes initially placed at different locations; (c) and (d) magnitude of configurational derivative against iteration count for holes placed at initial location 1 location 2 respectively.

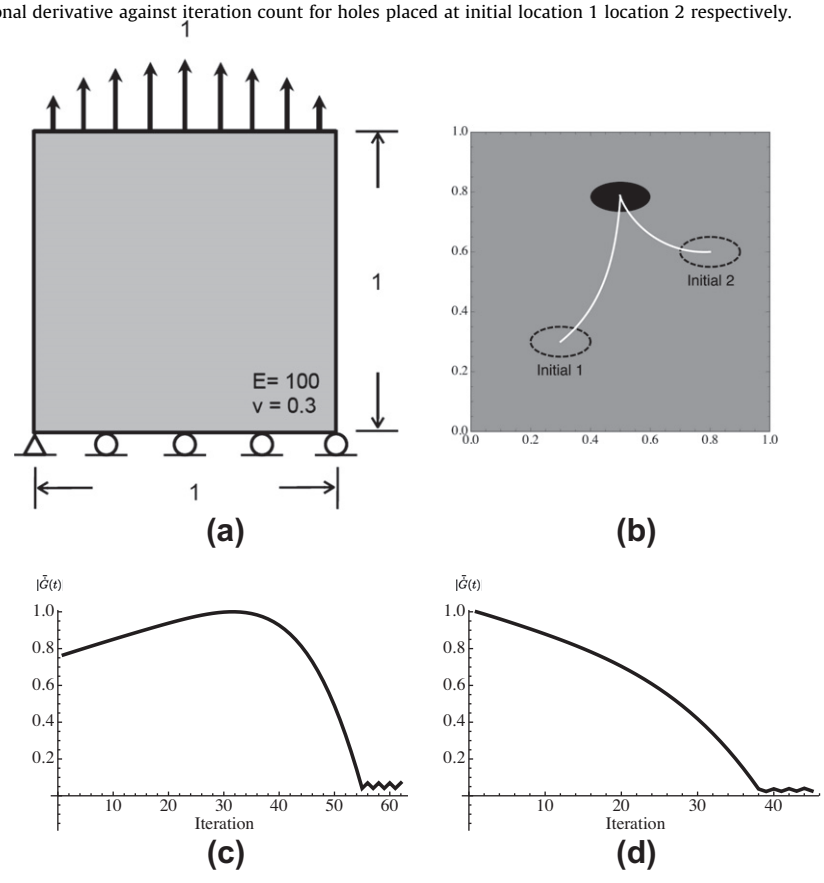

Fig. 16. Optimal location for inserting an elliptical inclusion ($E = 1000$) in a square plate: (a) quadratically distributed traction, (b) iterates of inclusions initially placed at different locations; (c) and (d) magnitude of configurational derivative against iteration count for inclusions placed at initial location 1 location 2 respectively.

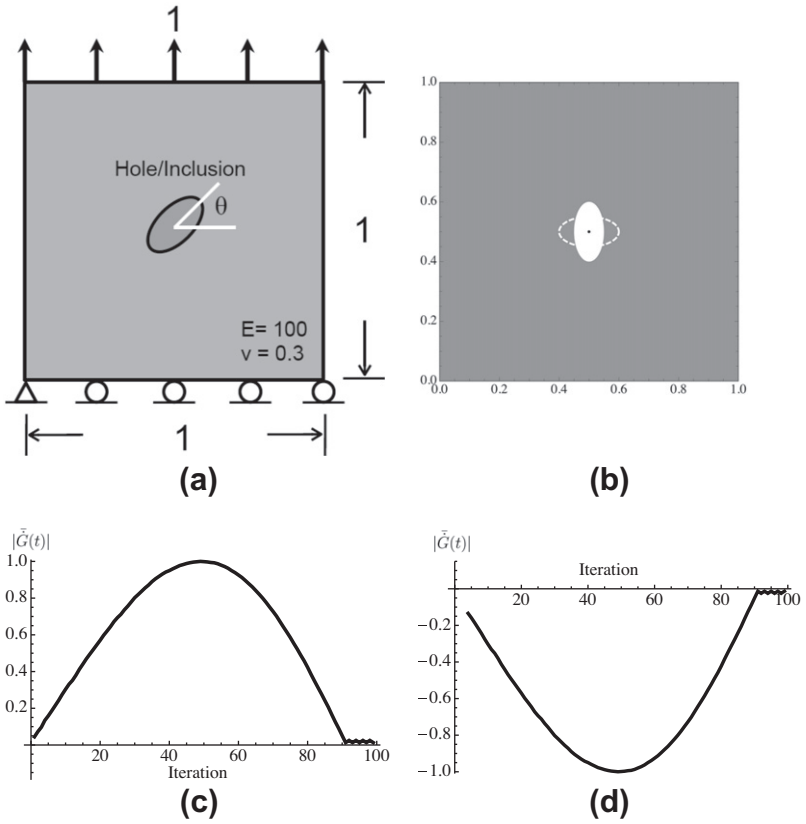

Fig. 17. Optimal orientation for an inserted elliptical hole in a square plate: (a) illustration of loading and boundary conditions for the hole orientation problem. (b) Optimal orientation; (c) and (d) magnitude of configurational derivative against iteration count for holes initially oriented with $\theta = 0^\circ$ and $\theta = 3^\circ$ respectively.

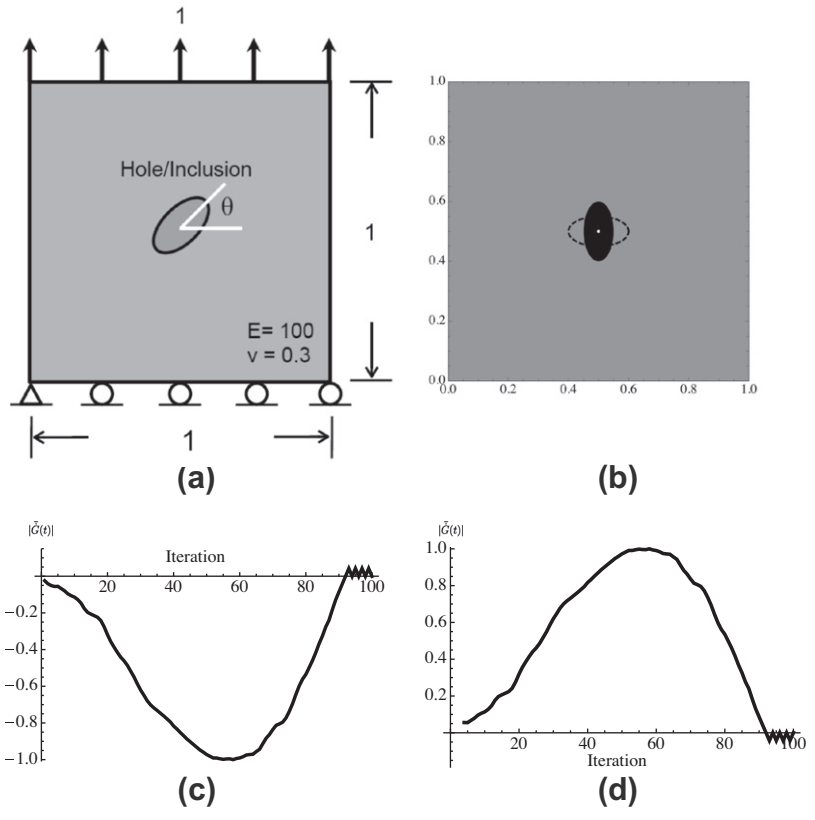

Fig. 18. Optimal orientation for an inserted elliptical inclusion ($E = 1000$) in a square plate: (a) illustration of loading and boundary conditions for the inclusion orientation problem, (b) optimal orientation; (c) and (d) magnitude of configurational derivative against iteration count for inclusions initially oriented with $\theta = 0^\circ$ and $\theta = -3^\circ$ respectively.

D.2. Optimal orientation of a heterogeneity

Next, we consider the optimal orientation of an inserted heterogeneity using the configurational derivative given in Eq. (15). The inserted hole and inclusion were initially placed at center of the plate as shown in Figs. 17(a) and 18(a). Here, we define θ as the orientation of the major axis of an elliptical feature. In this example as well, two initial orientations for the heterogeneity were considered. The orientation was iteratively updated using Eq. (15) until the optimal orientation was reached ($\theta = 90^\circ$ for both hole and inclusion), as illustrated in Figs. 17(b) and 18(b). It should be noted that while the absolute values of the configurational derivative were small both in horizontal and vertical orientations, the sign of the configurational derivative was such as to drive the heterogeneity towards the vertical orientation.

D.3. Optimal scaling of a heterogeneity

Once a heterogeneity is optimally placed and orientated in the plate, it can be uniformly scaled to its optimal size (for a chosen weight w on relative mass) using Eq. (17) as demonstrated next. We consider a hole/inclusion with major axis along the horizontal direction inserted at the center of a plate that is subjected to a uniform traction as shown in Fig. 17(a). The configurational derivatives of hole and inclusion as the ellipse is scaled are plotted in Fig. 19. In the figure, the axis corresponds to the semi-major diam-

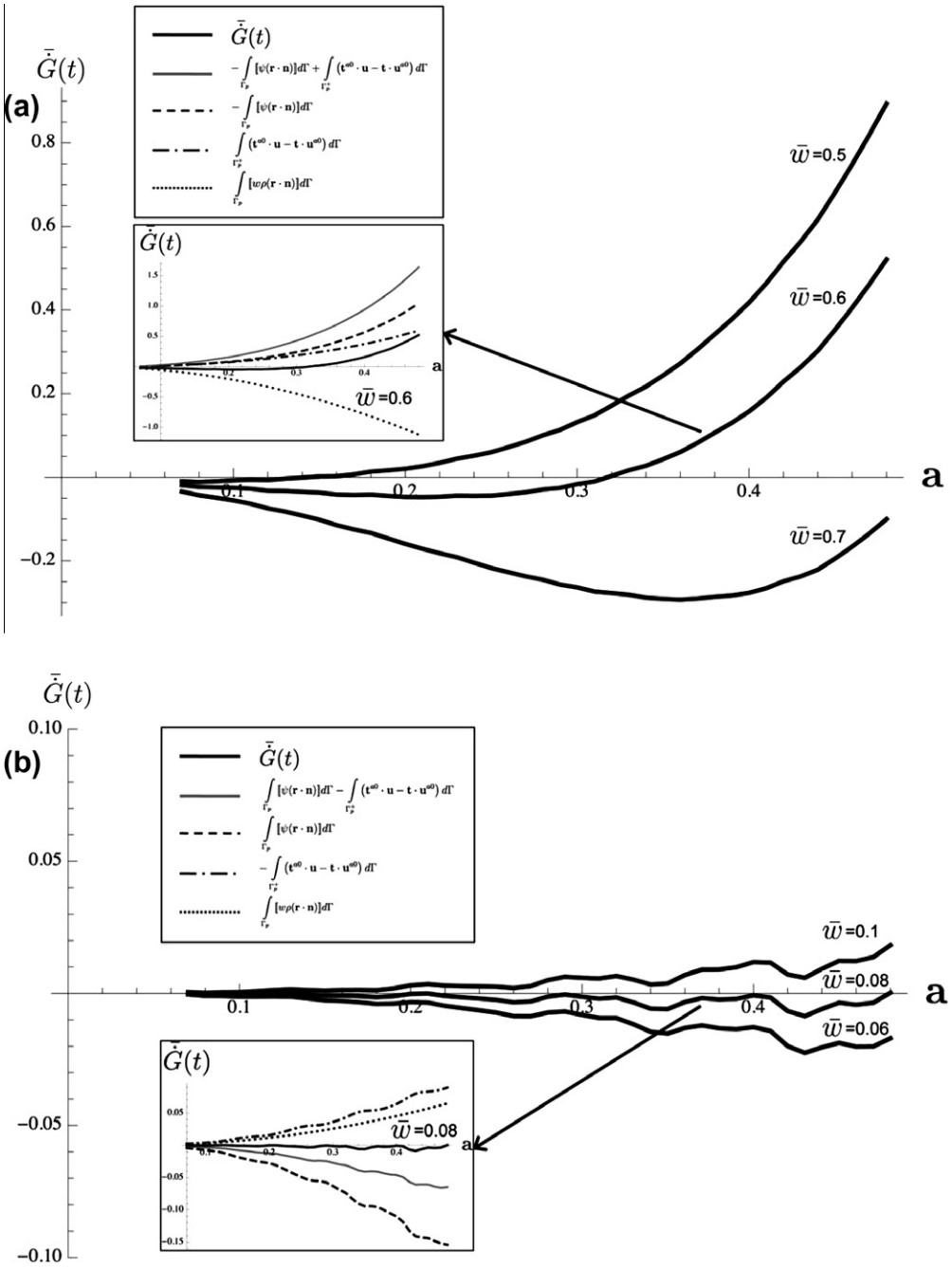

Fig. 19. Normalized configurational derivatives as a function of the semi-major diameter of elliptical heterogeneities inserted and scaled at the center of a plate ($\rho = 1$) subjected to uniaxial tension: (a) hole (b) inclusion ($\rho = 2$). All the plotted quantities are normalized with respect to the total compliance of homogeneous plate.

eter of the elliptical heterogeneity. The ordinate represents the value of the configurational derivative, and the plotted curves correspond to different choices of the weight $\bar{w}$ (defined here as $w = \frac{\bar{w}}{(1-\bar{w})}\frac{\bar{\psi}}{\bar{\rho}}$ with $\bar{w} \in [0, 1]$, and with $\bar{\psi}$ and $\bar{\rho}$ being scaling constants on ψ and ρ). The figures inset show the relative magnitudes of the various component terms in Eq. (17) for a specific weight value.

While the examples in Fig. 19 illustrate the procedure, the size of the heterogeneity in general depends nonlinearly on the chosen $\bar{w}$ and as a result, physically meaningful results (where features don't encompass the whole domain or shrink to zero size) may exist only for a limited range of the $\bar{w}$ values. This is particularly true for the inclusion, where only for a limited choice of the weight an optimal solution exists owing to the dominance of one of the objective terms at other weight values.

References

Ammari, H., Kang, H., 2005. Reconstruction of Small Inhomogeneities from Boundary Measurements. Lecture Notes in Mathematics, vol. 1846. Springer.

Amstutz, S., 2006. Sensitivity analysis with respect to a local perturbation of the material property. Asymptotic Analysis 49, 87–108.

Ansola, R., Canales, J., Tarrago, J., Rasmussen, J., 2002. An integrated approach for shape and topology optimization of shell structures. Computers and Structures 80, 449–458.

Arora, J., 1993. An exposition of the material derivative approach for structural shape sensitivity analysis. Computer Methods in Applied Mechanics and Engineering 105, 41.

Bendsoe, M., Sigmund, O., 2003. Topology Optimization. Springer, New York.

Bennett, J., Botkin, M. (Eds.), 1986. The Optimum Shape: Automated Structural Design. Plenum Press, NY.

Budiansky, B., Rice, J., 1973. Conservation laws and energy release rates. Journal of Applied Mechanics 40, 201–203.

Cea, J., Garreau, S., Guillaume, P., Masmoudi, M., 2000. The shape and topological optimizations connection. Computer Methods in Applied Mechanics and Engineering 188, 713–726.

Cedio-Fengya, D., Moskow, S., Vogelius, M., 1998. Identification of conductivity imperfections of small diameter by boundary measurements. Continuous dependence and computational reconstruction. Inverse Problems 14, 553–595.

Christensen, R., 2005. Mechanics of Composite Materials. Dover Publications, Mineola, NY.

Dems, K., Mroz, Z., 1983. Variational approach by means of adjoint systems to structural optimization and sensitivity analysis – I. International Journal of Solids and Structures 19, 677.

Dems, K., Mroz, Z., 1984. Variational approach by means of adjoint systems to structural optimization and sensitivity analysis – II. International Journal of Solids and Structures 20, 517.

Dems, K., Mroz, Z., 1986. On a class of conservation rules associated with sensitivity analysis in linear elasticity. International Journal of Solids and Structures 22, 737–758.

Eschenauer, H., Kobelev, V., Schumacher, A., 1994. Bubble method for topology and shape optimization of structures. Structural Optimization 8, 42–51.

Eshelby, J., 1956. The continuum theory of lattice defects. Progress in Solid State Physics, vol. 3. Academic Press, New York, p. 79.

Gopalakrishnan, S., Suresh, K., 2008. Feature sensitivity: a generalization of topological sensitivity. Finite Elements in Analysis and Design 44, 696–704.

Haug, E., Choi, K., Komkov, V., 1986. Design Sensitivity Analysis of Structural Systems. Academic Press, Orlando, FL.

Hughes, T., Cottrell, J., Bazilevs, Y., 2005. Isogeometric analysis: CAD, finite elements, NURBS, exact geometry and mesh refinement. Computer Methods in Applied Mechanics and Engineering 194, 4135–4195.

Kagan, P., Fischer, A., 2000. Integrated mechanically based CAE systems using B-spline based finite elements. Computer-Aided Design 32, 539.

Kang, H., Kim, K., 2007. Anisotropic polarization tensors for ellipses and ellipsoids. Journal of Computational Mathematics 25, 157–168.

Knowles, J., Sternberg, E., 1972. On a class of conservation laws in linearized and finite elastostatics. Archive for Rational Mechanics and Analysis 44, 187–211.

Kobelev, V., 2010. Òbubble-and-grainÓ method and criteria for optimal positioning inhomogeneities in topological optimization. Structural and Multidisciplinary Optimization 40, 117–135.

Lin, C., Chao, L., 2000. Automated image interpretation for integrated topology and shape optimization. Structural and Multidisciplinary Optimization 20, 125–137.

Malvern, L., 1969. Introduction to the Mechanics of a Continuum Medium. Prentice-Hall, Englewood Cliffs, NJ.

Natekar, D., Zhang, X., Subbarayan, G., 2004. Constructive solid analysis: a hierarchical, geometry-based meshless analysis procedure for integrated design and analysis. Computer-Aided Design 36, 473.

Nazarov, S., Sokolowski, J., 2003. Asymptotic analysis of shape functionals. Journal de Mathematique Pures et Appliquees 82, 125–196.

Nemat-Nasser, S., Hori, M., 1999. Micromechanics: Overall Properties of Heterogeneous Materials. Elsevier Science B.V., Amsterdam.

Novotny, A., Feijóo, R., Taroco, E., Padra, C., 2007. Topological sensitivity analysis for three-dimensional linear elasticity problem. Computer Methods in Applied Mechanics and Engineering 196, 4354–4364.

Novotny, A.A., Feijóo, R.A., Taroco, E., Padra, C., 2003. Topological sensitivity analysis. Computer Methods in Applied Mechanics and Engineering 192, 803–829.

Pironneau, O., 1984. Optimal Shape Design for Elliptic Systems. Springer-Verlag.

Rayasam, M., Srinivasan, V., Subbarayan, G., 2007a. CAD inspired hierarchical partition of unity constructions for NURBS-based, meshless design, analysis and optimization. International Journal for Numerical Methods in Engineering 72, 1452–1489.

Rayasam, M., Srinivasan, V., Subbarayan, G., 2007. Unified topology and shape design of multiscale, heterogeneous structures through compositional modeling of geometry, material and behavior. In: Proceedings of World Congress on Structural and Multi-disciplinary Optimization (WCSMO), pp. 1769–1778.

Renken, F., 1997. Optimization Analysis for Solder Joint Shape Prediction Using Finite Element and NURBS Surface Representation. Master's Thesis, University of Colorado, Boulder.

Renken, F., Subbarayan, G., 2000. NURBS-based solutions to inverse boundary problems in droplet shape prediction. Computer Methods in Applied Mechanics and Engineering 190, 1391–1406.

Rice, J., 1968. A path-independent integral and the approximate analysis of strain concentrations by notches and cracks. Journal of Applied Mechanics 35, 379–386.

Sokolowski, J., Zochowski, A., 1999. On the topological derivative in shape optimization. SIAM Journal of Control Optimization 37, 1251–1272.

Sokolowski, J., Zolesio, J.P., 1992. Introduction to Shape Optimization: Shape Sensitivity Analysis. Springer Series in Computational Mathematics, vol. 1. Springer-Verlag.

Tang, P., Chang, H., 2001. Integration of topology and shape optimization for design of structural components. Structural and Multidisciplinary Optimization 22, 65–82.

Zhang, X., Rayasam, M., Subbarayan, G., 2007. A meshless, compositional approach to shape optimal design. Computer Methods in Applied Mechanics and Engineering 196, 2130–2146.

Zhang, X., Subbarayan, G., 2004. A constructive approach for heterogeneous material modeling and analysis. Computer-Aided Design and Applications 1, 171–178.

Zhang, X., Subbarayan, G., 2006. jNURBS: an object-oriented, symbolic framework for integrated, meshless analysis and optimal design. Advances in Engineering Software 37, 287–311.